Cell Reports
Methods

Article

A kinetic fluorescence polarization ligand assay for monitoring BAX early activation

Graphical abstract

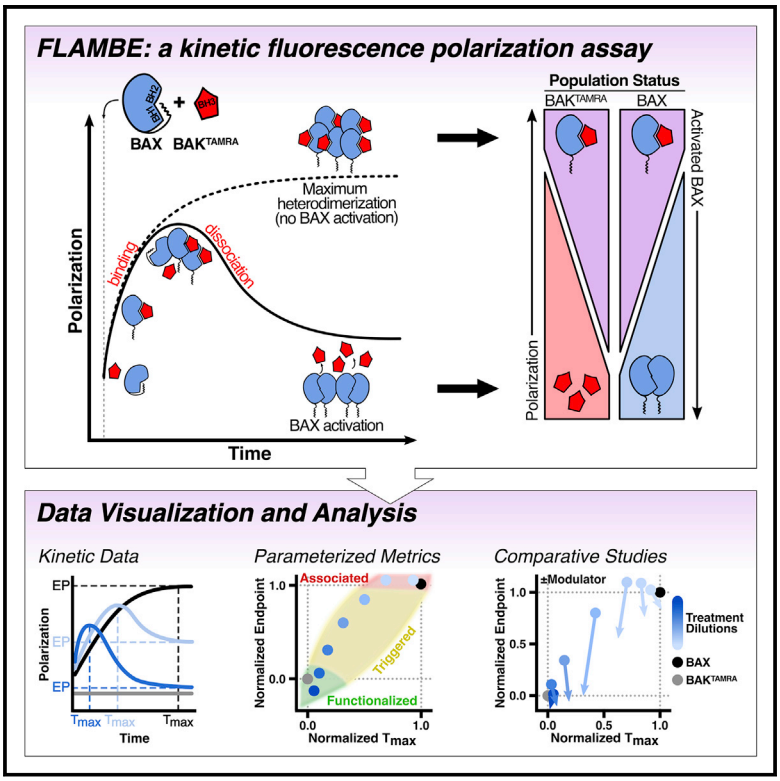

Highlights

- FLAMBE is a solution-based assay to measure the kinetics of monomeric BAX activation
- FLAMBE monitors BAX activation upstream of oligomerization and pore formation
- BAX activation by BH3-dependent or -independent mechanisms is detectable by FLAMBE
- FLAMBE integrates into workflows for screening and characterizing BAX modulators

Authors

Jesse D. Gelles, Jarvier N. Mohammed, Yiyang Chen, Tara M. Sebastian, Jerry Edward Chipuk

Correspondence

jerry.chipuk@mssm.edu

In brief

To study the real-time activation of BAX, Gelles et al. develop a kinetic fluorescence polarization ligand assay for monitoring BAX early activation (FLAMBE). Validation with a repertoire of BAX modulators and structural mutants, along with data parameterization methods, demonstrates the integration of FLAMBE within workflows for studying the mitochondrial pathway of apoptosis.

Gelles et al., 2022, Cell Reports Methods 2, 100174
March 28, 2022
https://doi.org/10.1016/j.crmeth.2022.100174

CellPress

Cell Reports Methods

CellPress
OPEN ACCESS

Article

A kinetic fluorescence polarization ligand assay for monitoring BAX early activation

Jesse D. Gelles,[1,2,3,4,7] Jarvier N. Mohammed,[1,2,3,4,6,7] Yiyang Chen,[1,2,3,4,6] Tara M. Sebastian,[1,4] and Jerry Edward Chipuk[1,2,3,4,5,6,8,*]

[1]Laboratory of Mitochondrial Biology in Human Health and Disease, Icahn School of Medicine at Mount Sinai, One Gustave L. Levy Place, New York, NY 10029, USA
[2]Department of Oncological Sciences, Icahn School of Medicine at Mount Sinai, One Gustave L. Levy Place, New York, NY 10029, USA
[3]Department of Dermatology, Icahn School of Medicine at Mount Sinai, One Gustave L. Levy Place, New York, NY 10029, USA
[4]The Tisch Cancer Institute, Icahn School of Medicine at Mount Sinai, One Gustave L. Levy Place, New York, NY 10029, USA
[5]The Diabetes, Obesity, and Metabolism Institute, Icahn School of Medicine at Mount Sinai, One Gustave L. Levy Place, New York, NY 10029, USA
[6]The Graduate School of Biomedical Sciences, Icahn School of Medicine at Mount Sinai, One Gustave L. Levy Place, New York, NY 10029, USA
[7]These authors contributed equally
[8]Lead contact
*Correspondence: jerry.chipuk@mssm.edu
https://doi.org/10.1016/j.crmeth.2022.100174

MOTIVATION *In vitro* BAX activation studies are invaluable platforms for studying cellular and pharmacological modulators of apoptosis. The gold standard for studying BAX function relies on membrane permeabilization assays, which assess the pore-forming activity of oligomeric BAX. However, there are currently no rapid or kinetic assays to interrogate real-time activation of monomeric BAX in solution, thereby limiting any molecular insights that occur upstream of mitochondrial permeabilization. Furthermore, available methods to observe the activation of monomeric BAX suffer from low throughput and static observations. To address this methodological gap, we developed FLAMBE, a kinetic fluorescence polarization-based assay to measure monomeric BAX activation in solution via concomitant displacement of a labeled peptide. This approach maintains the benefits of rapid kinetic data generation in a low-cost microplate format without requiring specialized equipment or large quantities of protein. FLAMBE compliments available experimental strategies and expands the accessibility of investigators to monitor early steps within the BAX activation continuum.

SUMMARY

Developmental, homeostatic, and pharmacological pro-apoptotic signals converge by activating the BCL-2 family member BAX. Studies investigating molecular regulation of BAX are commonly limited to methodologies measuring endpoint phenotypes and do not assess activation of monomeric BAX. Here, we present FLAMBE, a fluorescence polarization ligand assay for monitoring BAX early activation, that measures activation-induced release of a peptide probe in real time. Using complementary parallel and tandem biochemical techniques, we validate, corroborate, and apply FLAMBE to a contemporary repertoire of BAX modulators, characterizing their contributions within the early steps of BAX activation. Additionally, we use FLAMBE to reveal that historically "dead" BAX mutants remain responsive to activation as quasi-functional monomers. We also identify data metrics for comparative analyses and demonstrate that FLAMBE data align with downstream functional observations. Collectively, FLAMBE advances our understanding of BAX activation and fills a methodological void for studying BAX with broad applications in cell biology and therapeutic development.

INTRODUCTION

Thousands of pro-death cues are integrated into a single apoptotic mechanism that hinges upon BAX-mediated mitochondrial outer membrane permeabilization (MOMP). Native BAX is predominantly a soluble, inactive monomer due to the α9 helix occupying its own hydrophobic binding groove ("BC" groove) (Suzuki et al., 2000). In response to irreparable intrinsic cellular

stress, BAX is activated by BH3-only direct activator proteins, such as BIM, at a unique "trigger site" located at the N-terminal surface formed by the α1 and α6 helices (Gavathiotis et al., 2008). Triggering BAX elicits several structural changes, including displacement of the α1–α2 loop, exposure of key BH3 domain residues, and mobilization of the α9 helix from the BC groove (Gavathiotis et al., 2010), and consequent functional changes, such as association with the outer mitochondrial membrane (OMM) via the exposed α9 helix, oligomerization, and MOMP (Antonsson et al., 2000; Gross et al., 1998; Hsu et al., 1997). As such, the BAX activation continuum can be conceptually separated into an "activation" phase and an "execution" phase.

BAX activation studies fall into two classes: functional and biochemical. The former commonly measures membrane permeabilization (e.g., isolated mitochondria, biochemically defined liposomes) as a surrogate readout for activation (Kuwana et al., 2002; Luna-Vargas et al., 2019; Renault et al., 2013; Ryan and Letai, 2013; Schafer et al., 2009). While they are the gold standard, these assays do not reflect our growing understanding of BAX biology—namely, the intramolecular and large-scale structural rearrangements that convert BAX from an inactive cytosolic monomer into a membrane-associated oligomeric pore. Conversely, these activation steps are observable with biochemical methodologies (e.g., gel filtration, multimer crosslinking, non-denaturing gel electrophoresis), which involve significant sample processing, suffer from low throughput, and have limited temporal scope. As such, there is a need in the field for a rapid, high-throughput, kinetic approach for interrogating monomeric BAX activation.

Here, we describe a kinetic fluorescence polarization ligand assay for monitoring BAX early activation (termed FLAMBE), which measures the binding status of a fluorescently labeled BH3 peptide to BAX. We selected a fluorescence polarization (FP) technique, which has previously been validated as a suitable high-throughput, micro-format assay, to study molecular interactions with anti-apoptotic BCL-2 family proteins (Zhai et al., 2012; Zhang et al., 2002) (described in Figures S1A–S1E). Collectively, FLAMBE is a kinetic biochemical assay that retains the benefits of rapid data generation, minimal sample handling, and accessibility of use while advancing our conception of the BAX activation continuum by observing monomeric BAX activation. The ability to detect early-activation steps renders FLAMBE an ideal technical foundation for cell-biology investigations and small-molecule development in studies focused on the BCL-2 family.

RESULTS

Development of an FP assay for BAX

For our BAX activation assay, we selected a 5-Carboxytetramethylrhodamine (TAMRA)-labeled BAK-BH3 peptide (BAK^{TAMRA}) that forms non-productive BH3-in-groove interactions with BAX (Czabotar et al., 2013; Dewson et al., 2012). Like any FP assay, the binding of BAK^{TAMRA} to BAX results in an increased signal over time (a metric termed "Polarization", further detailed in Figure S1E), which, over time, eventually plateaus as the population forms the maximum number of heterodimers. We hypothesized that BAX activation, which results in structural rearrangement and multimerization, would displace the BAK^{TAMRA} probe and be visualized as a real-time concomitant decrease in Polarization (model shown in Figure 1A). Furthermore, the Polarization value of a sample would reflect the fraction of bound BAK^{TAMRA}, providing insights into the activation status of the BAX population (Figure 1A, right). To test our model, we measured Polarization over time in samples with increasing concentrations of BAX and observed a stepwise change in the kinetics of BAK^{TAMRA} binding and displacement from BAX (Figure 1B). BCL-2 family proteins predominately interact through BH3-in-groove interactions, and, therefore, we predicted that BAK^{TAMRA} was binding to the BAX BC groove. To validate this assumption, we tested two BC-groove mutants that potently inhibit BAX homodimerization and function, G108V and R109D (Czabotar et al., 2013; Dengler et al., 2019; Meijerink et al., 1998), but neither mutation ablated interactions with BAK^{TAMRA} (data not shown). Therefore, we generated a groove-occluded BAX mutant by introducing cysteine residues to form disulfide bonds between the BC groove and α9 helix ($BAX^{V83C,A112C,V177C,L185C}$ [BAX^{BC}]). Compared with wild-type (WT) or reduced BAX^{BC}, binding was completely abrogated with the oxidized BAX^{BC} mutant, indicating that BAK^{TAMRA} interacts at the BAX BC groove (Figure S1F).

A feature of BAX activation is the separation from direct-activator BH3 domains—the "hit and run" model—and we predicted that this would also apply to the BAK-BH3 peptide (Kim et al., 2009; Perez and White, 2000; Shamas-Din et al., 2014). To confirm that Polarization trends are due to a loss of BAX:BAK^{TAMRA} heterodimers, we replicated the conditions of the FP assay with fluorescently labeled BAX before subjecting samples to size-exclusion chromatography (SEC) and measuring elution fluorescence. At a BAX concentration that exhibited a signal plateau in a parallel FP, BAX co-eluted with BAK^{TAMRA}, indicating heterodimer formation (Figure 1C, "lo"). When we repeated this approach with a higher BAX concentration, we observed a complete loss of BAK^{TAMRA} co-elution, mirroring the loss of the Polarization signal in the FP assay (Figure 1C, "hi"). BAX exhibits concentration-dependent auto-activation (Gavathiotis et al., 2010; Tan et al., 2006), and BAK^{TAMRA} displacement could be from activation-induced structural rearrangements or subsequent multimerization. Of note, BAX eluted as a monomer, indicating that BAK^{TAMRA} dissociation was not due to dimerization-induced competition for the BC groove. However, the sample displayed a slight shift suggestive of activation-induced conformational changes. To validate that BAK^{TAMRA} dissociation resulted from BAX auto-activation, we crosslinked samples with disuccinimidyl suberate (DSS) following a BAX titration FP assay and generated oligomers indicative of active BAX (Figure 1D). Crosslinking analyses artificially promote oligomer formation of activated BAX, and so we confirmed BAX auto-activation in the presence of large unilamellar vesicles (LUVs) and observed dose-dependent permeabilization (Figure 1E). Collectively, these data demonstrate that an FP assay measuring BAK^{TAMRA} binding status serves as a surrogate for BAX activation.

FP assays detect real-time BAX activation in solution

As a proof-of-concept experiment, we investigated whether the kinetic FP assay could observe a common method to artificially

CellPress
OPEN ACCESS

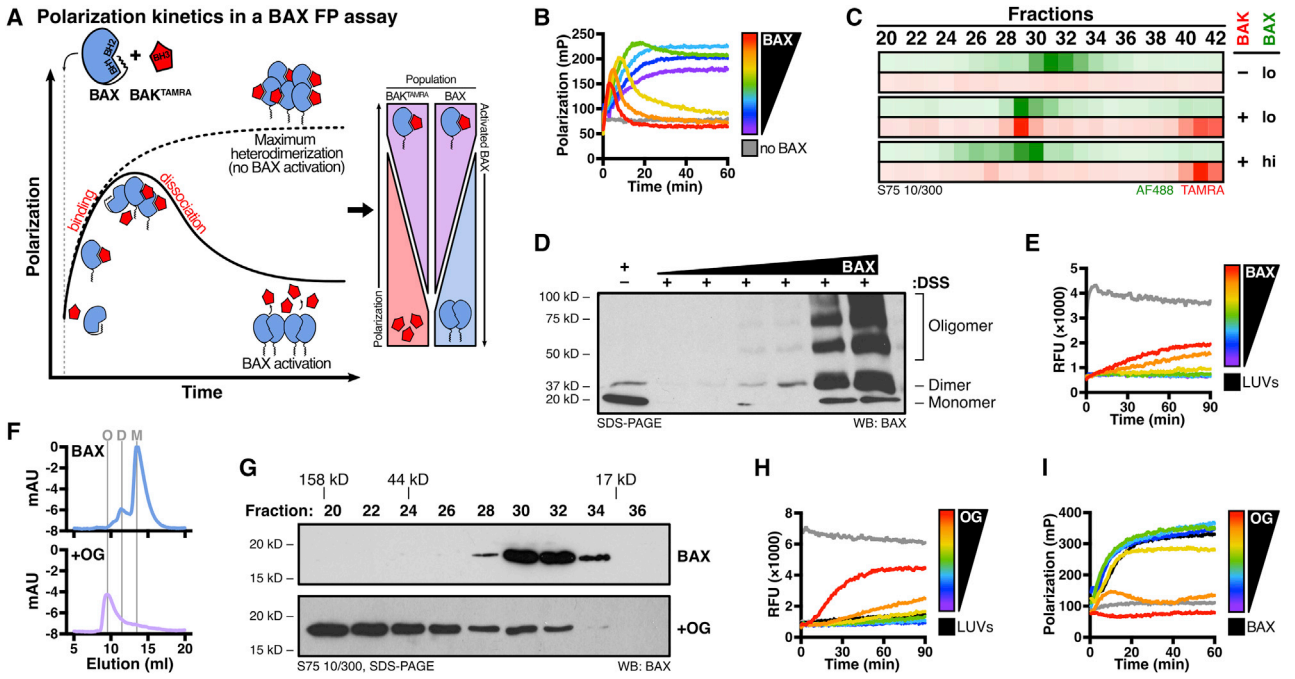

Figure 1. The kinetic FP assay is a high-throughput and rapid method to measure BAX activation in solution

(A) Illustration of kinetic Polarization trends resulting from the binding and dissociation of a TAMRA-labeled BAK-BH3 peptide (BAK^{TAMRA}) to BAX. Polarization increases as BAX binds BAK^{TAMRA} (dotted line); in conditions with BAX activation, real-time release of BAK^{TAMRA} results in a decreasing Polarization signal over time (solid line).

(B) BAK^{TAMRA} (50 nM) was added to BAX (42–125 nM), and Polarization was repeatedly measured for 1 h.

(C) Heatmap depicting fluorescence in SEC fractions of AF488-labeled BAX (lo: 90 nM; hi: 200 nM) and BAK^{TAMRA} (50 nM) following incubation at 25°C for 1 h to parallel the FP assay.

(D) DSS crosslinking and western blot analysis of samples following a BAX titration FP (16–500 nM). The BAX control from the highest concentration sample was treated with vehicle.

(E) Kinetics of LUV permeabilization by auto-activated BAX (4–250 nM).

(F) A280 absorption curves of BAX (2.4 μM) ± OG (0.7%) incubated at 4°C overnight and subjected to SEC. O, oligomer; D, dimer; M, monomer.

(G) Western blot detection of BAX within SEC fractions prepared as in (F).

(H) Kinetics of LUV permeabilization by BAX (75 nM) in the presence of OG (0.08%–0.24%).

(I) BAK^{TAMRA} (50 nM) was added to BAX (30 nM) in the presence of OG (0.0031%–0.1%) and subjected to the FP assay.

Gray data depict BAK^{TAMRA} (FP assays) or CHAPS (LUV assays) controls. Kinetic data are represented as mean.

See also Figure S1.

activate BAX with the detergent octyl-β-glucoside (OG) (Hsu and Youle, 1998). OG-activated BAX is traditionally achieved by incubation in supra-micellar OG concentrations followed by dilution and assessment of endpoint or functional outcomes (Antonsson et al., 2000; Kuwana et al., 2002). Indeed, this treatment method resulted in a predominately oligomeric BAX population without the requirement for a membrane (Figures 1F and 1G). Expectedly, the species formed by this activation strategy did not exhibit binding to BAK^{TAMRA} due to the distinct conformation of oligomeric BAX (data not shown). Therefore, we investigated whether the FP assay could observe real-time, OG-mediated activation at the monomeric stage. We utilized sub-micellar concentrations of OG that did not destabilize liposomes to facilitate parallel investigations between LUV and FP assays (<0.3%, established in Figure S1G). BAX treated with OG and immediately exposed to LUVs demonstrated dose-dependent activation (Figure 1H), and we confirmed that 0.25% OG could robustly functionalize BAX populations without prolonged incubation (Figure S1H compared with Figure 1E). Furthermore, we were able to capture the kinetics of this direct activator-like function of OG within the FP assay (Figure 1I). These data suggest that sub-micellar concentrations of OG generate active BAX monomers, which were not readily detected by prior methodologies (see discussion). By comparison, the kinetic BAX FP was sufficiently sensitive and specific to detect real-time BAX activation.

In the cell, BAX is activated through protein-protein interactions with BCL-2 family direct activators, and so we next tested our FP assay with a protein-mediated activation method. BIM primarily targets BAX at a distinct site formed by α1 and α6 (the trigger site) (Gavathiotis et al., 2008), which is distal to the canonical BC groove and therefore would not exhibit direct competition with the BAK^{TAMRA} probe. BAX treated with a BIM-BH3 (BIM^{BH3}) peptide exhibited a dose-dependent displacement of BAK^{TAMRA} at activating concentrations (Figure 2A). Polarization increased with low concentrations of BIM^{BH3}, which indicates an increase in the molecular size of

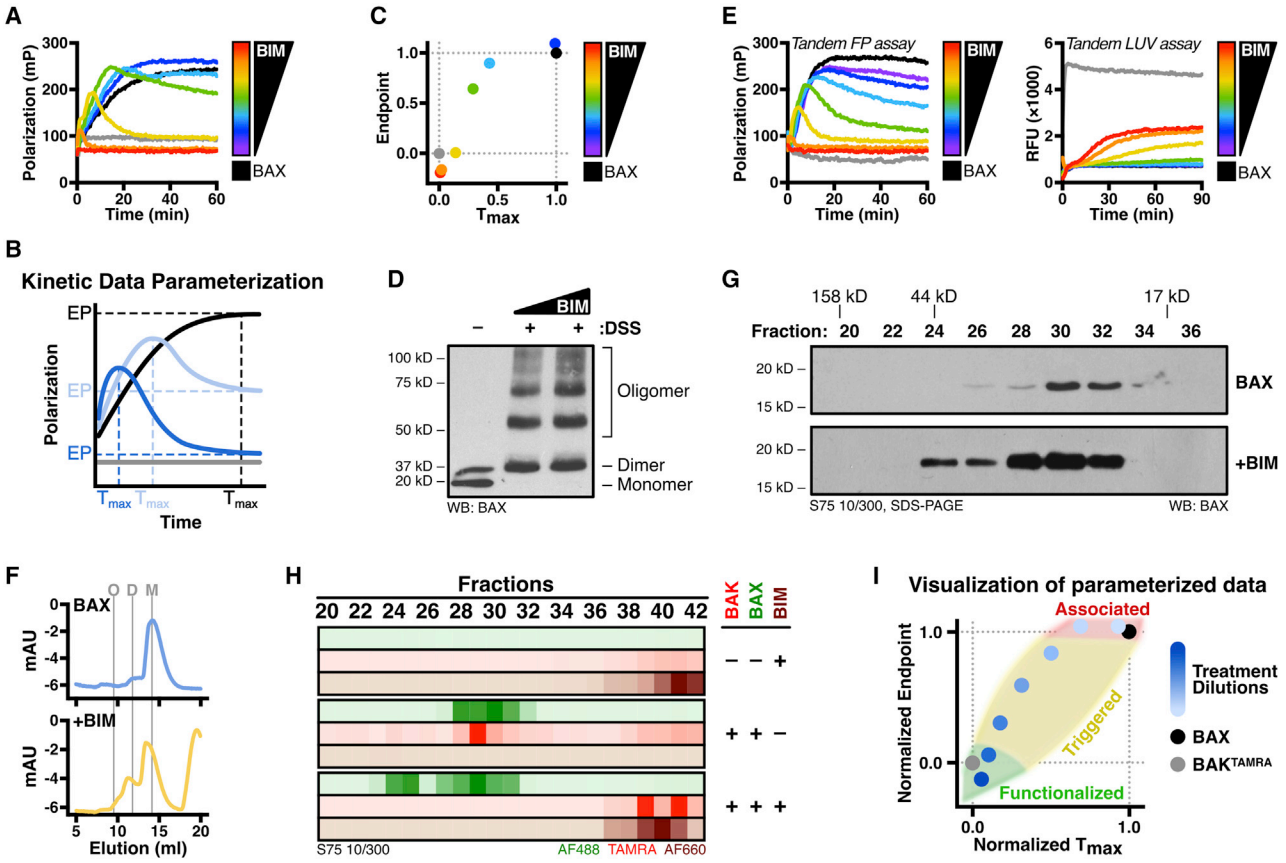

Figure 2. FLAMBE measures BAX activation upstream of functionalization by BIM

(A) FP assay of BAX (50 nM) in the presence of BIM^{BH3} (BIM, 0.08–2.5 μM).

(B) Diagram depicting parameterization of kinetic FP data by extracting two metrics: (1) endpoint Polarization (EP) signal and (2) time-to-maximum signal (T_{max}). Treatment conditions and BAX and BAK^{TAMRA} controls are represented by blue, black, and gray lines, respectively.

(C) Parameterization of FP data in (A) normalized to BAX and BAK^{TAMRA} controls.

(D) DSS crosslinking and western blot analysis of samples following a BIM^{BH3} titration FP (0.08–0.16 μM).

(E) FP assay of BAX (50 nM) in the presence of BIM^{BH3} (0.04–2.5 μM) (left). LUVs were added to samples and monitored for permeabilization (right).

(F) A280 absorption curves of BAX (2.4 μM) ± BIM (1:10 M excess) incubated overnight at 4°C and subjected to SEC. O, oligomer; D, dimer; M, monomer.

(G) Western blot detection of BAX within SEC fractions prepared as in (F).

(H) Heatmap depicting fluorescence in SEC fractions of AF488-labeled BAX (90 nM), AF660-labeled BIM^{BH3} (2.5 μM), and BAK^{TAMRA} (50 nM) following incubation at 25°C for 1 h to parallel the FP assay.

(I) Illustration depicting parameterized data falling into defined regions indicative of associated, triggered, or functionalized BAX in response to treatment.

BAK^{TAMRA} (50 nM) was added immediately prior to measurements for all FP assays. Gray data depict BAK^{TAMRA} (FP assays) or CHAPS (LUV assays) controls. Kinetic data are represented as mean.

See also Figure S2.

BAK^{TAMRA} and likely represents a BIM^{BH3}:BAX:BAK^{TAMRA} heterotrimer; stable, non-triggering BIM binding has been described at sub-activating concentrations (Tsai et al., 2015). Compared with endpoint FP assays, this assay captures the kinetics of BAX activation, providing investigators with additional informative metrics to measure BAX biology. We selected a dual-metric strategy to parameterize kinetic FP data, using both endpoint Polarization (EP) values and the timepoint of the maximum Polarization within the assay (T_{max}), which represents when the rate of BAK^{TAMRA} displacement outpaces association events (Figure 2B). Plotting normalized EP and T_{max} data provides a convenient method to observe the trend of BAX activation in response to the BIM titration (Figure 2C; see STAR Methods).

BAX is also activated by BID downstream of death receptor signaling (Li et al., 1998), and so we tested caspase-8-cleaved recombinant BID (C8-BID) in our assay. BAK^{TAMRA} was displaced from BAX in response to C8-BID, demonstrating dose-dependent changes in EP and T_{max}, and parallel LUV permeabilization studies confirmed BAX activation (Figures S2A–S2C). However, BID binds to the BAX BC groove (Czabotar et al., 2013; Wang et al., 1996), and therefore these FLAMBE data may be a combination of activation and direct competition effects. Additionally, C8-BID displayed some interaction with BAK^{TAMRA} in the absence of BAX, which may be due to BID's structural homology to multi-domain BCL-2 family proteins (Chou et al., 1999); by comparison, a BID-BH3 (BID^{BH3}) peptide

did not interact with BAK^{TAMRA} (Figures S2D and S2E). Interestingly, sub-activating concentrations of the BID^{BH3} peptide increased Polarization similar to BIM^{BH3}, indicating heterotrimerization and corroborating observations that the BID^{BH3} peptide may have increased affinity for the trigger site compared with the BID protein (Cartron et al., 2004; Dengler et al., 2019; Leshchiner et al., 2013) (Figure S2F). The preference of BID for either the BAX BC groove or trigger site and the relevance of cytosolic BID-mediated activation remain open questions in the field, and so we did not explore BID further in this work (see limitations of the study). As BIM is the predominant activator of BAX in the cell, we focused future FP experiments on BIM-mediated BAX activation (Sarosiek et al., 2013).

To assess whether the 2D graph could indicate underlying BAX biology, we investigated the state of BIM^{BH3}-treated BAX at the end of the FP assay using two methods. First, we subjected FP samples to crosslinking analysis and observed hallmark BAX laddering, indicative of activation (Figure 2D). However, crosslinking promotes oligomer formation, and so we next assessed BAX activity more specifically by adding LUVs to samples immediately following the FP assay and measuring permeabilization kinetics. In this FP-LUV tandem assay, only the BIM^{BH3} concentrations exhibiting rapid BAK^{TAMRA} dissociation were able to permeabilize LUVs, albeit after a temporal lag (Figure 2E). Importantly, the BAK^{TAMRA} control had no effect on LUVs (data not shown), and it has been demonstrated that pores are formed by BAX homo-oligomers (Antonsson et al., 2001; Sundararajan and White, 2001), confirming that BAK^{TAMRA} had no role in LUV permeabilization. To determine the progression of BIM-induced BAX activation within the FP assay, we subjected BIM^{BH3}-treated BAX to SEC and observed a significant, but minority, population of BAX dimers but no oligomers (Figures 2F and 2G). SEC of samples replicating the FP assay with fluorescently labeled BAX and BIM^{BH3} revealed a complete loss of co-elution despite BAX remaining mostly monomeric (Figure 2H). These data indicate that BIM-triggered BAX remains primed in solution until stabilizing influences by membranes facilitate oligomerization and pore formation. Therefore, we can approximate whether the BAX population is activated (release of BAK^{TAMRA}, "triggered") or sufficiently primed to exhibit functional hallmarks (such as membrane permeabilization, "functionalized") using parameterized data from the FP assay (Figure 2I). Since the FP assay detected BAX activation in response to triggering, but distinct from oligomerization, we named our assay FLAMBE (FP ligand assay for measuring BAX early-activation).

FLAMBE captures early-activation steps of BAX upstream of structural rearrangements and oligomerization

Our proof-of-concept experiments inspired us to reconsider the meaning of "activated BAX," and so we sought to evaluate functionally impaired mutants of BAX with FLAMBE. A historically dead BAX mutant ($BAX^{C62S,V121C,C126S,I136C}$ [BAX^{4M}]) can be oxidized to introduce a disulfide tether between α5 and α6, which prevents structural rearrangements required for MOMP (Czabotar et al., 2013). Oxidized (locked) BAX^{4M} was unable to permeabilize LUVs in response to the BIM^{BH3} peptide or C8-BID, even at supra-physiological concentrations (Figures 3A and 3B). Importantly, reduced (unlocked) BAX^{4M} was proficient at LUV permeabilization in response to activating conditions, performing comparably to BAX containing the background cysteine-to-serine mutations ($BAX^{C62S,C126S}$ [BAX^{C2}]) (Figures S3A–S3C). Unexpectedly, locked BAX^{4M} treated with OG exhibited some function at high BAX concentrations. Furthermore, while exhibiting no oligomerization in response to BIM^{BH3}, locked BAX^{4M} formed oligomeric species when incubated with supra-micellar OG (Figures 3C, 3D, and S3D).

The inability of BAX^{4M} to permeabilize membranes or form oligomers is what led to the determination that it is a "non-activating" structural mutant. However, BAX^{4M} has been shown to retain binding affinity for BH3 domains (Czabotar et al., 2013), and, therefore, we used FLAMBE to investigate whether BAX^{4M} can be triggered. Both the locked and unlocked BAX^{4M} forms exhibited binding and displacement of BAK^{TAMRA} in a dose-dependent manner (Figures S3E and S3F). Locked BAX^{4M} titrated with BIM^{BH3} or with sub-micellar OG demonstrated BAK^{TAMRA} displacement similar to the unlocked ("activatable") mutant, indicating a trigger-mediated response and not off-pathway dimerization as previously reported (Garner et al., 2016) (Figures 3E, 3F, S3G, and S3H). To reconcile these observations, we performed a tandem FP-LUV assay to sequentially observe the progression of BAX activation. While locked BAX^{4M} exhibited intramolecular rearrangement sufficient to displace BAK^{TAMRA}, it was unable to mature into pore-forming units, as demonstrated by the lack of LUV permeabilization (Figure 3G). In contrast, OG-induced BAX^{4M} oligomers were unobservable within FLAMBE but exhibited functionality in the presence of LUVs (Figure 3H). These data reveal that BAX^{4M} remains responsive to triggering (i.e., exhibiting activation steps captured by FLAMBE) and that the inability to undergo large-scale structural rearrangement (i.e., domain swapping) prevents functionalization.

Prior to domain swapping, BAX undergoes several hallmark structural steps in response to triggering (Gavathiotis et al., 2010; Kim et al., 2009), and so we utilized a panel of incremental loss-of-function mutants to identify which steps are critical for FLAMBE detection (Figure 4A). Working back from oligomerization, we first utilized a disulfide tether mutant that prevents α9 mobilization and disrupts BAX translocation to membranes ($BAX^{A112C,V177C}$ [$BAX^{\alpha9}$]). The locked $BAX^{\alpha9}$ mutant exhibited no response to direct activators and only permeabilized LUVs in a dose-dependent manner; the unlocked form of the mutant remained sensitive to activation (Figures 4B, 4C, and S4A). A structural step preceding α9 mobilization is the repositioning of the flexible loop between α1 and α2, which can be disrupted by introducing a disulfide tether between the loop and α6 ($BAX^{L45C,M137C}$ [$BAX^{\ell1-2}$]) (Gavathiotis et al., 2010). Compared with the unlocked control, loop-locked BAX was inert in response to direct activators, even at saturating BAX concentrations (Figures 4D, 4E, and S4B). Finally, we selected a recently identified trigger site mutant reported to impair BAX activation (BAX^{I133A}) and confirmed that it remained inert in response to BIM^{BH3} and C8-BID (Figures 4F and 4G) (Dengler et al., 2019). Of note, each loss-of-function mutant demonstrated increased LUV permeabilization at supra-physiological concentrations when treated with OG (Figures 4B, 4D, and 4F). As with the

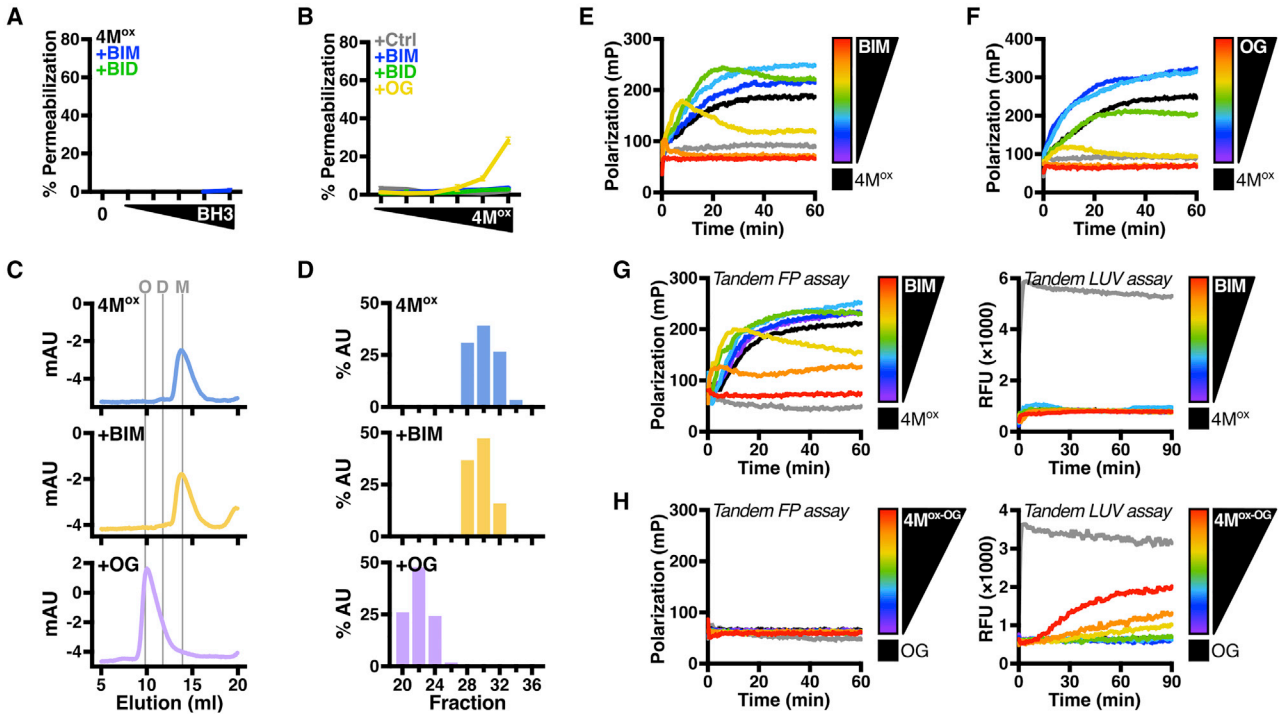

Figure 3. FLAMBE reveals that a non-oligomerizing BAX mutant exhibits early-activation responses to BIM

(A and B) Normalized endpoint LUV permeabilization by oxidized BAX^{4M} ($4M^{ox}$).

(A) $4M^{ox}$ (100 nM) was treated with a titration of BIM^{BH3} (BIM, 0.08–2.5 μM) or C8-BID (BID, 8–250 nM).

(B) Several concentrations of $4M^{ox}$ (8–250 nM) were treated with BIM^{BH3} (2.5 μM), C8-BID (250 nM), or OG (0.25%).

(C and D) A280 absorption curves and western blot quantification (Figure S3D) of $4M^{ox}$ (2.4 μM) ± BIM^{BH3} (1:10 M excess) or OG (0.7%) incubated overnight at 4°C and subjected to SEC.

(E and F) FP assay of $4M^{ox}$ (30 nM) in the presence of (E) BIM^{BH3} (0.08–2.5 μM) or (F) OG (0.008%–0.25%).

(G) FP assay of $4M^{ox}$ (100 nM) in the presence of BIM^{BH3} (0.04–2.5 μM) (left) followed by addition of LUVs and monitored for permeabilization (right).

(H) OG-activated BAX^{4M} ($4M^{ox-OG}$, 8–500 nM) was subjected to tandem FP-LUV assays as in (G). $4M^{ox-OG}$ BAX was produced by incubation at 4°C overnight in 0.7% OG to generate oligomers.

BAK^{TAMRA} (50 nM) was added immediately prior to measurements for all FP assays. Gray data depict BAK^{TAMRA} (FP assays) or CHAPS (LUV assays) controls. Kinetic data are represented as mean; error bars denote SD.

See also Figure S3.

locked BAX^{4M} mutant, these results indicate that OG-mediated BAX activation may not be defined by the same structural events and is dependent on the BAX concentration to properly oligomerize (see discussion).

We tested each BAX mutant within FLAMBE to confirm binding with BAK^{TAMRA} and selected non-activating concentrations for future experiments with BIM^{BH3} (Figures S4C and S4D). In response to BIM^{BH3}, the unlocked mutants both activated and demonstrated a release of BAK^{TAMRA} with similar sensitivity (Figure S4E). Interestingly, FLAMBE revealed that BIM^{BH3}-induced BAK^{TAMRA} release was not abolished by any of the loss-of-function mutations (Figure 4H). In an attempt to disrupt triggering directly, we tested another trigger site mutant of BAX (BAX^{K21E}) but still observed an activation profile in response to BIM^{BH3} (Figure S4F); this result, in conjunction with more recent investigations, may suggest an alternative mechanism for BAX^{K21E} (see discussion). The BIM^{BH3}-activation assays were all conducted with BAX concentrations determined by titration experiments (Figures S4C and S4D), but this strategy may have camouflaged mutant-specific differences in BIM sensitivity. Therefore, we did a direct comparison FLAMBE experiment using each mutant at the same concentration without and with BIM^{BH3} (Figures S4G–S4I). At a concentration in which WT BAX slightly activates in response to BIM^{BH3}, the locked mutants (BAX^{4M}, $BAX^{\alpha 9}$, and $BAX^{\ell 1-2}$) exhibited reduced baseline BAK^{TAMRA} binding and activation by BIM^{BH3}, while BAX^{I133A} performed similarly to WT (Figures 4I and 4J). Parameterizing and comparing data from these FLAMBE experiments revealed that trends clustered the mutants into two groups: BIM-associated and BIM-triggered mutants (Figure 4K). Collectively, these experiments reveal that FLAMBE measured an early step of BAX activation and was not impeded by the disruption of previously described structural events. Furthermore, solution-based activation studies conducted with FLAMBE provide investigators with a method to uncouple our definition of BAX activation from functional outcomes.

FLAMBE provides additional insights into emerging modulators of BAX activation

So far, we have demonstrated that the FLAMBE technique is a highly sensitive method to monitor BAX early activation without

CellPress
OPEN ACCESS

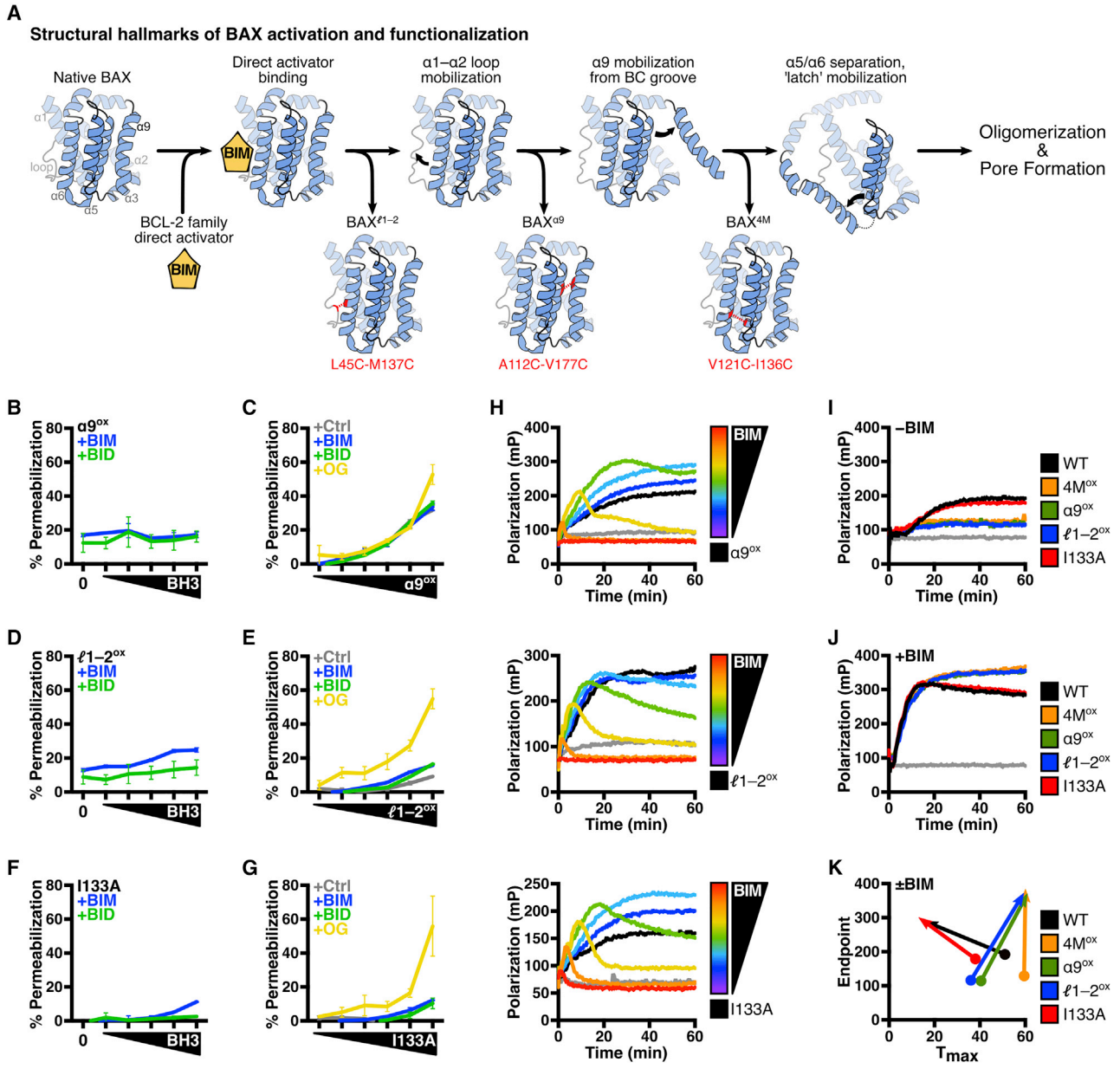

Figure 4. FLAMBE captures BIM-mediated triggering distinct from pore-forming activity in functionally impaired mutants of BAX

(A) Illustration of defined structural hallmarks along the BAX activation continuum. Several double-cysteine mutants have been described to disrupt these structural events by tethering BAX with disulfide bonds and preventing BAX functionalization (noted in red).

(B and C) Normalized endpoint LUV permeabilization by α9-locked BAX ($\alpha9^{ox}$).

(B) $\alpha9^{ox}$ (60 nM) was treated with a titration of BIM^{BH3} (BIM, 0.08–2.5 μM) or C8-BID (BID, 8–250 nM).

(C) Several concentrations of $\alpha9^{ox}$ (8–250 nM) were treated with BIM^{BH3} (0.25 μM), C8-BID (250 nM), or OG (0.25%).

(D and E) ℓ1–2 loop-locked BAX ($\ell1–2^{ox}$) treated as in (B) and (C) at either (D) a single concentration (125 nM) or (E) several concentrations (8–250 nM).

(F and G) Experiments using BAX^{I133A} (I133A) with concentrations and treatments as in (D) and (E).

(H) FLAMBE assay with $\alpha9^{ox}$ (125 nM, top), $\ell1–2^{ox}$ (125 nM, middle), and I133A (50 nM, bottom) in the presence of BIM^{BH3} (0.08–2.5 μM).

(I and J) Comparative screen of BAX loss-of-function mutants (60 nM) by FLAMBE revealed differences in (I) BAK^{TAMRA} binding and (J) response to BIM^{BH3} (0.5 μM).

(K) Parameterization of FLAMBE data from (I) and (J) summarized as arrows depicting responses to BIM^{BH3} treatment.

BAK^{TAMRA} (50 nM) was added immediately prior to measurements for all FP assays. Gray data depict the BAK^{TAMRA} in FP assays. Kinetic data are represented as mean; error bars denote SD.

See also Figure S4.

a requirement for downstream functional outcomes. Therefore, we leveraged these benefits to investigate several recently described modulators of BAX activity. The detergent *n*-dodecyl-phosphocholine (DDPC, called "Fos-12" in referenced work) can generate homogeneous and functional BAX oligomers following prolonged incubation at supra-micellar concentrations (i.e., 3 mM DDPC, incubated at 4°C overnight) (Hauseman et al., 2020). Since our experiments with OG revealed different activation mechanisms and kinetics between supra- and sub-micellar approaches, we hypothesized that DDPC may similarly exhibit a real-time effect on BAX. To test if DDPC could activate BAX at sub-micellar concentrations (<1.5 mM), we incubated BAX overnight with DDPC and observed a population shift toward oligomeric BAX in the absence of a membrane, which was not observed for BIM^{BH3}-treated BAX prepared using the same method (Figure 5A). Compared with the original study, this treatment strategy did not generate homogeneous oligomers but was sufficient to induce a shift in more than 70% of the BAX population (Figures 5B and S5A; see discussion). Furthermore, native gel electrophoresis revealed a dose-dependent shift toward oligomeric BAX at concentrations below the critical micelle concentration (CMC) (Figure 5C). To test the functionality of DDPC-induced oligomers, we treated BAX with sub-micellar DDPC overnight (BAX^{DDPC}) and observed dose-dependent LUV permeabilization in response to the functionalized BAX (Figure 5D). However, FLAMBE experiments with BAX^{DDPC} demonstrated no interactions with BAK^{TAMRA} (data not shown), which aligns with the observation that oligomeric BAX^{DDPC} does not retain several interaction sites compared with the monomeric species (Hauseman et al., 2020).

While overnight incubation with DDPC was required to generate functionalized BAX, we hypothesized that FLAMBE would detect the real-time activation of BAX monomers in response to DDPC. BAX treated with DDPC exhibited immediate dose-dependent activation, as measured by FLAMBE, but did not exhibit concomitant LUV permeabilization (Figures 5E and S5C). Furthermore, SEC experiments mimicking the FLAMBE assay revealed that BAX remained predominantly monomeric in response to DDPC despite the dissociation of BAK^{TAMRA}; this outcome was dissimilar to OG-treated BAX, which generated high-molecular-weight species under the same conditions (Figure 5F). Comparisons with BIM- and OG-treated BAX suggested a distinct mechanism of DDPC activation, which we interrogated using loss-of-function mutants. While locked BAX^{4M} readily oligomerized in response to DDPC, the oligomers did not correspond to functionality and minimally permeabilized LUVs (Figures 5G and S5D–S5F). Additionally, DDPC treatment of $BAX^{\alpha 9}$ and $BAX^{\ell 1-2}$ exhibited reduced permeabilization compared with their unlocked controls (Figures 5G and S5G). Considering these data, we leveraged the ability of FLAMBE to sensitively detect changes in BAX activation kinetics and demonstrated that sub-activating concentrations of BIM^{BH3} and DDPC could synergize and potentiate BAX activation (Figures 5H and 5I). These experiments show how real-time activation detected by FLAMBE can further characterize BAX biology using conditions and treatments that are not possible with assays measuring endpoint functional outcomes.

Since FLAMBE detects trends in monomeric BAX activation, alone or in conjunction with a direct activator, we reasoned that FLAMBE would be well suited for studies investigating pharmacological interventions of the BAX activation continuum. Therefore, we investigated three recently described BAX activation modulators that target an allosteric pocket formed by the $\alpha 3$–$\alpha 4$ and $\alpha 5$–$\alpha 6$ loops (Figure 6A). BIF44 (4-phenoxyphenol) was reported to synergize with BIM-induced MOMP (Pritz et al., 2017), and, indeed, we observed an increase in LUV permeabilization when BIM-activated BAX was co-treated with BIF44 (Figure 6B). Kinetic data revealed that BIF44 increased both the maximum and the rate of permeabilization following BIM^{BH3} activation, indicating that BAX permeabilized more LUVs (Figures S6A and S6B). Using FLAMBE, we demonstrated that BIF44 binds to BAX in the absence or presence of BIM^{BH3} but likely exhibits more binding specificity in BIM-primed samples (Figures S6C and S6D). Interestingly, FLAMBE experiments revealed a more complete population activation at each BIM^{BH3} concentration, but the kinetics of BAK^{TAMRA} association and dissociation (T_{max}) were mostly unaffected (Figures 6C and S6E). These results suggested that BIF44 augments functionalization by promoting activated monomer maturation but not by affecting triggering. This led us to hypothesize that BAX may be forming more productive multimers prior to membrane association. To test this hypothesis, we co-treated BAX with BIM^{BH3} and BIF44, performed SEC, and observed a substantial increase of dimeric species in solution compared with either single treatment (Figures 6D and S6F). Additionally, the synergistic effect of BIF44 was limited by the degree of BIM^{BH3}-mediated activation (Figure S6G). Collectively, these data demonstrate that the synergistic effect of BIF44 occurs at the active monomer stage of the BAX continuum and promotes permeabilization by facilitating productive multimerization prior to membrane association.

Next, we investigated a BAX inhibitor, BAI1, which robustly inhibited LUV permeabilization by BAX functionalized via auto-activation or direct activators (Figure 6E). It was suggested that BAI1 binding stabilized core residues and prevented structural rearrangements during activation (Garner et al., 2019); therefore, we utilized FLAMBE to investigate whether the inhibitory effects of BAI1 were upstream of membrane-associated functional phenotypes. BAI1 did not inhibit BAK^{TAMRA} dissociation from BAX undergoing auto-activation or activated by BIM^{BH3} (Figures S6H and S6I). When we titrated BAI1 onto BAX, we observed dose-dependent increases in Polarization, which then converged upon the addition of a sub-activating concentration of BIM^{BH3} (Figure 6F). These data reveal promiscuous binding of BAI1 at high concentrations, but binding became more selective by BIM triggering (see discussion). When we treated BAX with concentrations of BAI1 that abolished LUV permeabilization, we observed no changes in the response to BIM^{BH3} within FLAMBE (Figures 6G and S6J). These data suggest that the inhibitory effect of BAI1 occurs during activation steps downstream of the FLAMBE observational window, between activation-induced intramolecular rearrangements and larger conformational changes prior to, or at, the membrane. Ongoing efforts with this or other pharmacological agents will be enhanced by the

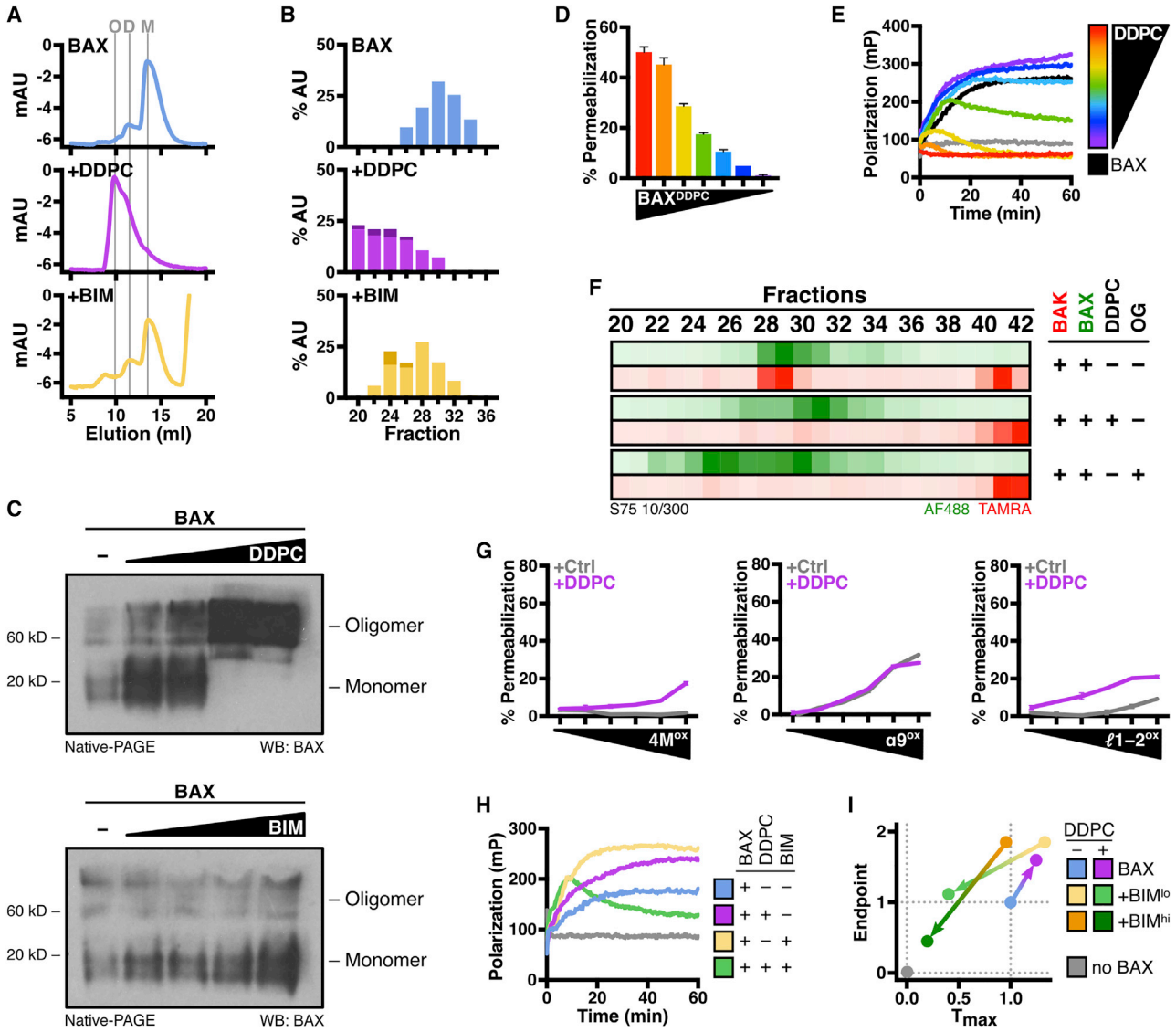

Figure 5. FLAMBE detects DDPC-mediated activation prior to oligomerization

(A and B) A280 absorption curves and western blot quantification (Figure S5A) of BAX (2.4 μM) ± DDPC (0.05–1 mM) or BIM^{BH3} (1:10 M excess) incubated overnight at 4°C and subjected to SEC. Darker bars denote signals from dimer bands.

(C) Native-PAGE analysis of BAX (100 ng) following overnight incubation at 4°C with DDPC (0.05–1 mM) or BIM^{BH3} (1:0–1:10 M excess).

(D) Normalized endpoint LUV permeabilization by DDPC-activated BAX (BAX^{DDPC}, 4–250 nM). BAX^{DDPC} was produced by incubating BAX with DDPC (1 mM) overnight at 4°C.

(E) FLAMBE assay of BAX (30 nM) in the presence of DDPC (0.008–0.5 mM).

(F) Heatmap depicting fluorescence in SEC fractions of AF488-labeled BAX (90 nM) and BAK^{TAMRA} (50 nM) treated with DDPC (1 mM) or OG (0.7%) following incubation at 25°C for 1 h to parallel the FP assay.

(G) Normalized endpoint LUV permeabilization by $4M^{ox}$ (8–250 nM, left), $\alpha9^{ox}$ (8–250 nM, middle), and $\ell1–2^{ox}$ (8–250 nM, right) treated with DDPC (1 mM) overnight at 4°C.

(H) FLAMBE assay of BAX (30 nM) in the presence of DDPC (31 μM) ± BIM^{BH3} (0.31 μM).

(I) Parameterization of FLAMBE data in (H) with additional BIM^{BH3} concentration (lo: 0.31 μM; hi: 0.63 μM).

BAK^{TAMRA} (50 nM) was added immediately prior to measurements for all FP assays. Gray data depicts the BAK^{TAMRA} in FP assays. Kinetic data are represented as mean; error bars denote SD.

See also Figure S5.

inclusion of methods such as FLAMBE, which will enable investigators to dichotomize mechanisms of action occurring at early- or late-stage BAX activation.

There have been increasing efforts to identify cellular modulators of BAX activation beyond BCL-2 family interactions, including post-translational modifications, bioactive lipids, and

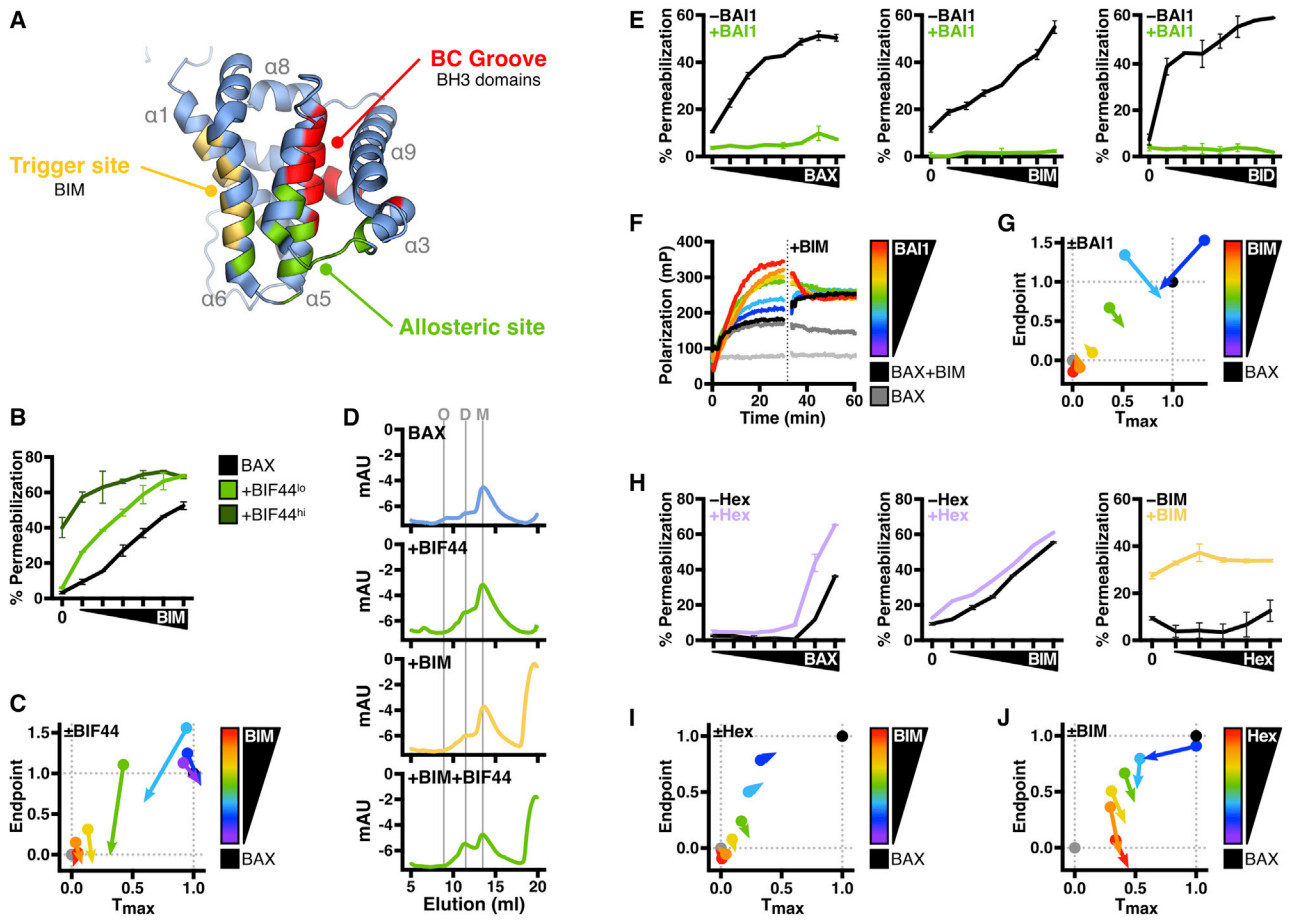

Figure 6. FLAMBE studies provide insights into the mechanism of BAX modulators targeting the allosteric site

(A) BAX structure (PDB: 2K7W; BIM SAHB helix not shown) highlighting interaction sites targeted by the reagents used within this work: trigger site (yellow), targeted by BIM; BC groove (red), targeted by BH3 domains and BAK^{TAMRA}; allosteric site (green), targeted by BIF44, BAI1, and hexadecenal.

(B) Normalized endpoint LUV permeabilization by BAX (75 nM) in the presence of BIM^{BH3} (0.08–2.5 μM) and BIF44 (lo: 250 μM; hi: 500 μM).

(C) Comparison of parameterized FLAMBE data (Figure S6E).

(D) A280 absorption curves of BAX (2.4 μM) ± BIM^{BH3} (1:10 M excess) ± BIF44 (250 μM) incubated for 1 h and subjected to SEC.

(E) Normalized endpoint LUV permeabilization by BAX ± BAI (25 μM). Left: BAX titration (100–1,000 nM), middle: BAX (75 nM) activated by BIM^{BH3} (0.04–2.5 μM), and right: BAX (75 nM) activated with C8-BID (4–250 nM).

(F) FLAMBE assay of BAX (50 nM) in the presence of BAI1 (1.5–50 μM). After 30 min, BIM^{BH3} (0.31 μM) was added to samples, and readings continued for another 30 min.

(G) Comparison of parameterized FLAMBE data (Figure S6J).

(H) Normalized endpoint LUV permeabilization of BAX treated with BIM^{BH3} and 2*t*-hexadecenal (Hex). Left: BAX (4–250 nM) ± Hex (125 μM), middle: BAX (100 nM) with BIM^{BH3} (0.08–2.5 μM) ± Hex (125 μM), and right: BAX (100 nM) in the presence of Hex (8–125 μM) ± BIM^{BH3} (160 nM).

(I and J) Comparison of parameterized FLAMBE data from (I) Figure S6K or (J) Figures S6L and S6M.

Gray data depict BAK^{TAMRA} controls in FP assays. Kinetic data are represented as mean; error bars denote SD.

See also Figure S6.

interactions with the OMM milieu (Frohlich et al., 2014; Mignard et al., 2014; O'Neill et al., 2016; Renault et al., 2015; Vasquez-Montes et al., 2021). However, these investigations are often limited to BAX-membrane interactions, and, therefore, the consequences on cytosolic BAX remain difficult to isolate. As an example, the sphingolipid metabolite 2*t*-hexadecenal (hexadecenal) was identified to regulate BAX, and recent work demonstrated that hexadecenal covalently modifies the BAX allosteric site, resulting in increased membrane permeabilization (Chipuk et al., 2012; Cohen et al., 2020). We assessed hexadecenal-induced activation in solution by treating BAX prior to direct activator or membrane exposure. In these experiments, we observed hexadecenal-mediated synergy with activating conditions; however, the effect was limited by the activating effect of BIM^{BH3} (Figure 6H). To investigate whether hexadecenal synergizes with BIM activation upstream of membranes, we utilized FLAMBE activation studies with varying concentrations of either BIM^{BH3} or hexadecenal. While BAX treated with sub-activating concentrations of hexadecenal demonstrated no change in sensitivity to BIM^{BH3} activation, BAX did exhibit synergy in a

hexadecenal-dependent manner when co-treated with sub-activating BIM^{BH3} (Figures 6I, 6J, and S6K–S6M). These data indicate that BAX must first be primed by BIM^{BH3} for the activating effects of hexadecenal to be revealed. By providing a window into BAX early-activation steps, FLAMBE is superior at measuring synergistic sequential binding of BAX modulators in solution and provides greater resolution of relevant BAX biology compared with previously available methodologies.

DISCUSSION

FLAMBE is a rapid solution-based approach to measure the kinetics of monomeric BAX activation

In response to activation, BAX is converted from cytosolic monomers to membrane-integrated oligomers. However, it remains debated whether multimerization of BAX occurs in the cytosol, the OMM, or both (Czabotar et al., 2013; Garner et al., 2016; Subburaj et al., 2015; Sung et al., 2015). The lack of consensus can be explained, in part, by differences in methodology and activating conditions. During this work, the addition of FLAMBE to the panel of BAX activation assays has led to several observations that deepen our understanding of BAX biology and may inform future efforts to regulate or pharmacologically target BAX. We will highlight these observations below and discuss the conclusions that can be drawn from the data.

Investigations describing solution oligomerization are frequently conducted by SEC and use detergents to activate or stabilize BAX (Antonsson et al., 2000; Gavathiotis et al., 2012; Reyna et al., 2017). OG activation has historically been conducted at concentrations above the CMC (~0.6%), and it is thought that protein-micelle interactions result in BAX activation (Ivashyna et al., 2009; Kuwana et al., 2002). Data from our studies suggested that while oligomerization required micellar OG, sub-micellar concentrations generated active monomers. Therefore, reliance on oligomerization to measure BAX activation overlooks monomer activation and selects for more heavy-handed treatment approaches. Similarly, DDPC-induced BAX oligomers required either supra-micellar concentrations and/or prolonged incubation (Hauseman et al., 2020). Detecting monomeric activation with FLAMBE revealed that DDPC activated BAX in real time and at concentrations that did not result in population shifts or LUV permeabilization. This observation inspired investigations into the synergistic activity of DDPC and BIM on BAX activation, which would not have been detectable using prior methods but was observed using FLAMBE. These results suggest a biphasic mechanism of detergent-activated BAX: sub-micellar detergent exhibits a real-time, direct-activator effect on monomeric BAX, while supra-micellar concentrations replicate the stabilizing influences of membranes and promote BAX oligomerization in solution. This concept has previously been suggested for the detergent CHAPS, which has exhibited concentration-dependent differential effects on BAX (Yao et al., 2014), and may be related to a recent finding that BAK oligomers bind and complex with lipids and detergents (Cowan et al., 2020).

Interestingly, BIM^{BH3}-mediated BAX activation remained mostly monomeric with a minority dimer population; oligomers were only detected when assisted by crosslinkers or membranes. This observation may explain why activated BAX exhibited a lag in our tandem LUV assays. BAX and BIM^{BH3} were incubated for an hour during the FLAMBE assay prior to the addition of LUVs; however, activated BAX permeabilized LUVs with the same kinetics as a traditional LUV assay without prior incubation. Collectively, these data suggest that BIM-activated BAX molecules only progress as far as the dimer stage in solution and is rate limited by the ability to undergo large-scale structural changes in the presence of membranes. Additionally, the tandem FLAMBE-LUV assays revealed different sensitivities for observing activated BAX, where LUVs did not permeabilize at concentrations exhibiting robust activation in FLAMBE. One explanation for this could be that FLAMBE detects single-molecule BAX activation within a population while LUV assays require a substantial population to be active for pore generation and detectable signal. We anticipate that the sensitivity of FLAMBE for detecting BAX activation will make it a valuable addition in investigators' biochemical toolbelts.

Using FLAMBE to study the activation phase advances our understanding of BAX structural biology

The steps within the BAX activation continuum have been interrogated by loss-of-function mutants, but characterization is often not fully explored due to a reliance on methods observing only the execution phase of BAX. While the structural mutants explored in this work did not permeabilize LUVs in response to BIM or BID, each exhibited pore formation when supra-physiological concentrations were treated with sub-micellar OG. Perhaps most strikingly, BAX^{4M}—a mutant engineered to ablate BAX oligomerization—completely oligomerized and permeabilized LUVs following incubation with OG above its CMC. These data suggest that detergent-mediated activation of BAX is perpetuated via a different set of structural events and may not be directly comparable to BH3-mediated BAX activation. By comparison, DDPC treatment oligomerized BAX^{4M} but did not potentiate LUV permeabilization, highlighting that BAX oligomerization is not synonymous with functionalization. Experiments with these mutants suggest that the steps of the BAX activation continuum are not conserved between physiological (e.g., peptide-mediated) and non-physiological (e.g., detergents) methods of activation, and therefore it may not be prudent to rely solely on detergent-mediated activation models for interrogations into underlying BAX biology.

We observed that the locked $BAX^{\alpha 9}$ mutant permeabilized LUVs at supra-physiological concentrations. The α9 helix is important for BAX translocation and interaction with the OMM, but its role in BAX oligomerization is unclear, and most structural investigations study BAX without the C-terminal helix (commonly a 21-residue truncation [$BAX^{\Delta C21}$]). $BAX^{\Delta C21}$ exhibits poor LUV permeabilization, which can be compensated by using supra-physiological concentrations or DDPC (Hauseman et al., 2020). In contrast, the locked $BAX^{\alpha 9}$ mutant was unresponsive to DDPC. It is theorized that activated BAX monomers propagate through BH3-in-groove symmetric dimers and that the α9 helix may play a role in pore formation (Dewson et al., 2012; Zhang et al., 2016); therefore, the ability of locked $BAX^{\alpha 9}$ to readily permeabilize LUVs in a BIM- or BID-independent manner was unexpected. One explanation may be that the disulfide bond in $BAX^{\alpha 9}$

disrupts full-range mobilization (thus weakening interactions with membranes) but does not completely occlude the BAX BC groove, which is supported by the observation that locked $BAX^{\alpha 9}$ still binds BAK^{TAMRA}. Similarly, previously reported BAX BC-groove mutants that do not form homodimers, G108V and R109D, retained the ability to bind, and then release, BAK^{TAMRA} within FLAMBE (data not shown). These results suggest that the various functions of the BAX BC groove (i.e., α9 sequestering, BH3 binding, dimerization) utilize unique residue signatures, making the topology of the groove more nuanced than previously thought.

Within our FLAMBE assays, each of the locked mutants (BAX^{4M}, $BAX^{\alpha 9}$, and $BAX^{\ell 1-2}$) remained responsive to BIM activation, albeit slightly attenuated compared with WT. These results suggested that activation-induced BAK^{TAMRA} displacement is not dependent on the mobilization of either the α1–α2 loop or the α9 helix. Additionally, the unlocked mutants displayed different activation sensitivities within our FLAMBE experiments. Most notably, the unlocked $BAX^{\alpha 9}$ mutant was extremely sensitive to BIM activation, which may be a consequence of the reduced cysteine residues weakening the affinity of the α9 helix to reside in the BC groove. Collectively, activation phase studies using FLAMBE have deepened our understanding of these structural mutants, which will continue to inform ongoing studies of BAX within the field. We believe that incorporating early-activation investigations into future BAX studies will help investigators differentiate between activation and functionalization, and avoid generalized conclusions stemming from specific techniques to study BAX.

Structural determinants of BAX interactions or activation are dichotomized by FLAMBE studies

Based on previous interpretations, we hypothesized that the trigger site mutants BAX^{I133A} and BAX^{K21E} would disrupt BIM^{BH3} triggering and selected them as negative controls for FLAMBE studies. While both mutants had impaired function (i.e., LUV permeabilization), FLAMBE assays revealed a conserved response to BIM^{BH3} in apparent contradiction with the reputation of these mutants. Here, we provide perspectives that may explain these unexpected results and encourage us to reconsider the widely held hypotheses of how these mutations disrupt BAX function.

BAX^{I133A} was discovered through a mutagenesis screen and demonstrated impaired crosslinking with recombinant BID and activation (Dengler et al., 2019). However, interaction studies were conducted in a P168G/W170A background, which alters α9 behavior and instigates interactions between BID and the trigger site (Schinzel et al., 2004). BAX NMR structures suggest that (1) I133 faces the BAX core during BIM binding and is unlikely to impact BIM interactions (PDB: 2K7W) (Gavathiotis et al., 2008) and (2) I133 may interact with the α1–α2 loop and stabilize a closed-loop conformation of inactive BAX (PDB: 1F16) (Gavathiotis et al., 2010; Suzuki et al., 2000). The latter model is strengthened by the observation that BAX^{I133A} exhibited a proteinase K digestion pattern indicative of an open-loop conformer. While I133 resides within the trigger site, there is no direct evidence that the mutation disrupts BIM interactions, and the impairment of BID-induced activation may suggest a more universal inhibition in BAX activation. One hypothesis is that I133 has a role in trigger-induced core rearrangements and the deficiency of BAX^{I133A} arises from a disrupted response to BH3 binding.

BAX^{K21} was identified as the residue exhibiting the largest chemical shift upon BIM^{BH3} peptide binding, and mutagenesis of the residue disrupted BIM-mediated oligomerization and apoptosis, collectively leading to the conclusion that BAX^{K21E} disrupted BIM binding (Gavathiotis et al., 2008). However, it was later reported that BAX^{K21E} was also less responsive to auto-activation instigated by a BAX^{BH3} peptide or heat, and loss of function was rescued via a complementary mutation in the BAX BH3 domain (Gavathiotis et al., 2010). The latter study revealed that active BAX self-perpetuates within the population using its own BH3 domain to trigger inactive monomers. Taken together, these studies suggest that BAX^{K21E} impairs BAX function by disrupting interactions between active and inactive BAX monomers and inhibiting perpetuation, not by disrupting BIM^{BH3} triggering directly. This interpretation explains why the BAX^{K21E} mutant remained responsive to BIM^{BH3} in our FLAMBE studies despite its initial reputation for disrupting interactions with BIM.

Assays measuring phenotypic outcomes cannot readily differentiate between loss of function due to defects in BH3 binding, triggering, structural events, translocation to membranes, multimerization, or pore formation. As such, studies limited by these methods may result in incomplete or ambiguous conclusions regarding the role of specific BAX residues. While we believe that the reputation of these mutants may be frequently mischaracterized, we demonstrate how FLAMBE studies, in conjunction with current methods to measure BAX function, will aid in the characterization of loss-of-function mutations and the specific determination of residues critical for BAX activation biology.

FLAMBE provides a platform for screening and characterizing small-molecule modulators of BAX

BAX is the primary mediator of the intrinsic pathway of apoptosis, and therefore efforts to identify small molecules that directly modulate BAX activity have profound therapeutic potential in several disease etiologies (Amgalan et al., 2020; Bove et al., 2014; Niu et al., 2017; Reyna et al., 2017; Xin et al., 2014). Limiting high-throughput screens and mechanistic investigations to membrane permeabilization assays risks excluding candidates that target specific BAX conformers along the activation continuum prior to the execution phase. Indeed, we observed evidence of this principle during our investigations of the BAX modulators that target the allosteric site. BIF44 and hexadecenal demonstrated a dependence on BIM to reveal any synergistic activation, indicating that these activators primarily operate on a conformer of BAX following triggering. BIF44 was previously shown to induce flexibility in the α1–α2 loop and partial exposure of the BAX BH3 domain, but how this related to BIM-mediated activation was not identified (Pritz et al., 2017). Here, we demonstrated that BIF44 accelerates BIM-induced BAX activation and multimerization during the activation phase, resulting in more productive pore formation during the execution phase. Similarly, FLAMBE studies revealed that the synergistic effect of hexadecenal occurs during BAX activation, prior to a requirement for membranes or oligomerization, which was not readily apparent in previous studies.

BAI1 was identified as a potent inhibitor of BAX, and we utilized FLAMBE to demonstrate that it did not affect triggering or dissociation of BAK^{TAMRA}, indicating that the inhibitory effect of BAI1 occurs at a later step within the BAX activation continuum. Our FLAMBE studies also revealed that, at concentrations ablating BAX function, BAI1 exhibited promiscuous binding to BAX, which corroborated a peripheral observation that BAI1 may exhibit alternative binding modalities in saturating conditions (Garner et al., 2019). The decrease in Polarization upon BIM addition suggests that BIM binding may either occlude these alternative low-specificity sites or promote uniform binding by increasing accessibility to the allosteric site of BAX. One interesting hypothesis is that BAX:BIM heterodimerization, but not necessarily activation, is sufficient to promote more selective binding of BAI1 to the BAX allosteric site (Tsai et al., 2015), though it is currently unclear what contribution promiscuous BAI1 binding has to the potent inhibition of BAX oligomerization and pore formation.

These studies example how FLAMBE will inform the interrogation and interpretation of candidate small molecules acting on monomeric BAX. Additionally, our observations imply that FLAMBE is capable of assessing non-apoptotic functional consequences of BAX that would not be detected in permeabilization assays. This aspect of FLAMBE may provide critical insights for future small-molecule screens by contextualizing results from cell-based assays when BAX interacts with proteins beyond the BCL-2 family. Moreover, we anticipate that FLAMBE will be a valuable technique for investigations into BH3-independent mechanisms by providing a method to study cytosolic BAX behavior prior to OMM interactions. We are encouraged by these various applications of FLAMBE and believe that it may ignite investigations into the ''moonlighting'' aspects of BAX biology.

Limitations of the study

While FLAMBE represents an advanced technique in the repertoire of assays to study BAX function, it is not without its limitations. FLAMBE data are generated by measuring real-time changes in Polarization (Figure S1E). As such, more rapid read intervals generate richer kinetic data. This restricts the number of samples that can be measured per assay without compromising the density of data acquisition. Additionally, the rapid kinetics of BAK^{TAMRA} binding and release restricts the number of confident replicates to duplicates (see STAR Methods). Therefore, a greater experimental N is required to determine reproducibility of results.

The use of BAK^{TAMRA} as a biologically relevant reporter to study BAX biology is also accompanied by certain constraints. BAK^{TAMRA} is predicted to bind to the BAX BC groove (Figure S1F), but we do not discount that the unstructured nature of the BAK^{TAMRA} peptide may contribute flexibility in the binding kinetics, affinity, or location on BAX. BAK^{TAMRA} is particularly useful for activation studies with BIM but may be less suited for agents targeting the BC groove, such as BID, which will exhibit direct competition (see Figure S2). However, we anticipate that FLAMBE could be adapted for such studies by using a different labeled probe.

Our FLAMBE observations are based in our understanding of the intramolecular rearrangements of triggered BAX. Importantly, the release of BAK^{TAMRA} represents a surrogate readout for these rearrangements but is not a *de facto* measurement of structural changes. The precise mechanism of trigger-induced BAK^{TAMRA} release remains unknown; similarly, the mechanism of activation-induced α9 mobilization remains poorly understood. We anticipate that future studies of signal propagation across the BAX structure will aid in contextualizing FLAMBE observations.

FLAMBE is extremely relevant for investigations into solution and cytosolic regulators of BAX activity. However, half of the BAX activation continuum involves downstream multimeric species or the mitochondrial membrane. We cannot disregard the cellular contributors that regulate, or molecular agents that may target, these late-stage steps of BAX functionalization, which would not be observable by FLAMBE (e.g., OMM milieu contributions). Despite this, FLAMBE was intended to complement current investigative workflows by characterizing the contributions, or lack thereof, of BAX regulators within the early steps of BAX activation. Therefore, we maintain that the integration of FLAMBE into the methodological toolbelt expands the technical foundation for cell-biology investigations and small-molecule development in BH3-dependent and -independent mechanisms of BAX activation.

STAR★METHODS

Detailed methods are provided in the online version of this paper and include the following:

- KEY RESOURCES TABLE
- RESOURCE AVAILABILITY
  - Lead contact
  - Materials availability
  - Data and code availability
- EXPERIMENTAL MODEL AND SUBJECT DETAILS
  - Bacterial cell lines
- METHOD DETAILS
  - Site-directed mutagenesis
  - BAX purification, recombinant proteins, and peptides
  - Fluorescence polarization assay and data parameterization
  - Large unilamellar vesicle (LUV) permeabilization assays
  - Cross-linking, gel electrophoresis, and immunoblotting
  - Size-exclusion chromatography and quantification of band intensities
  - Fluorescent gel filtration experiments
  - BAX structure visualization and annotation
- QUANTIFICATION AND STATISTICAL ANALYSIS

SUPPLEMENTAL INFORMATION

Supplemental information can be found online at https://doi.org/10.1016/j.crmeth.2022.100174.

ACKNOWLEDGMENTS

This work was supported by NIH grants R01 CA259110 (J.E.C.) and R01 CA206005 (J.E.C.), the JJR Foundation, the William A. Spivak Fund, the

Fridolin Charitable Trust, an American Cancer Society Research Scholar Award, a Leukemia & Lymphoma Society Career Development Award, and an Irma T. Hirschl/Monique Weill-Caulier Trust Research Award. This work was also supported in part by two research grants (5FY1174 and 1FY13416) from the March of Dimes Foundation, a Collaborative Pilot Award from the Melanoma Research Alliance, a Developmental Research Pilot Project Program within the Department of Oncological Sciences at the Icahn School of Medicine at Mount Sinai, and the Tisch Cancer Institute Cancer Center support grant (P30 CA196521). The authors wish to thank Drs. Thibaud T. Renault and Mark P.A. Luna-Vargas for their assistance in the development of the assays used within this work; Dr. Evripidis Gavathiotis for providing the $BAX^{\alpha 9}$, $BAX^{\alpha 1-2}$, and BAX^{K21E} plasmids; and Dr. James LaBelle for his aid and expertise with BH3 peptides.

AUTHOR CONTRIBUTIONS

Conceptualization, J.D.G., J.N.M., and J.E.C.; methodology, J.D.G. and T.M.S.; investigation, J.D.G., J.N.M., and Y.C.; writing, J.D.G., J.N.M., and J.E.C.; resources, J.N.M. and Y.C.; visualization, J.D.G.; funding acquisition, J.E.C.; supervision: J.E.C.

DECLARATION OF INTERESTS

The authors declare no competing interests.

Received: September 7, 2021
Revised: December 20, 2021
Accepted: February 2, 2022
Published: March 9, 2022

REFERENCES

Amgalan, D., Garner, T.P., Pekson, R., Jia, X.F., Yanamandala, M., Paulino, V., Liang, F.G., Corbalan, J.J., Lee, J., Chen, Y., et al. (2020). A small-molecule allosteric inhibitor of BAX protects against doxorubicin-induced cardiomyopathy. Nat. Cancer *1*, 315–328.

Antonsson, B., Montessuit, S., Lauper, S., Eskes, R., and Martinou, J.C. (2000). Bax oligomerization is required for channel-forming activity in liposomes and to trigger cytochrome c release from mitochondria. Biochem. J. *345*, 271–278.

Antonsson, B., Montessuit, S., Sanchez, B., and Martinou, J.C. (2001). Bax is present as a high molecular weight oligomer/complex in the mitochondrial membrane of apoptotic cells. J. Biol. Chem. *276*, 11615–11623.

Asciolla, J.J., Renault, T.T., and Chipuk, J.E. (2012). Examining BCL-2 family function with large unilamellar vesicles. J. Vis. Exp. *68*, 4291.

Bird, G.H., Gavathiotis, E., LaBelle, J.L., Katz, S.G., and Walensky, L.D. (2014). Distinct BimBH3 (BimSAHB) stapled peptides for structural and cellular studies. ACS Chem. Biol. *9*, 831–837.

Bove, J., Martinez-Vicente, M., Dehay, B., Perier, C., Recasens, A., Bombrun, A., Antonsson, B., and Vila, M. (2014). BAX channel activity mediates lysosomal disruption linked to Parkinson disease. Autophagy *10*, 889–900.

Cartron, P.F., Gallenne, T., Bougras, G., Gautier, F., Manero, F., Vusio, P., Meflah, K., Vallette, F.M., and Juin, P. (2004). The first alpha helix of Bax plays a necessary role in its ligand-induced activation by the BH3-only proteins Bid and PUMA. Mol. Cell *16*, 807–818.

Chipuk, J.E., McStay, G.P., Bharti, A., Kuwana, T., Clarke, C.J., Siskind, L.J., Obeid, L.M., and Green, D.R. (2012). Sphingolipid metabolism cooperates with BAK and BAX to promote the mitochondrial pathway of apoptosis. Cell *148*, 988–1000.

Chou, J.J., Li, H., Salvesen, G.S., Yuan, J., and Wagner, G. (1999). Solution structure of BID, an intracellular amplifier of apoptotic signaling. Cell *96*, 615–624.

Cohen, D.T., Wales, T.E., McHenry, M.W., Engen, J.R., and Walensky, L.D. (2020). Site-dependent cysteine lipidation potentiates the activation of proapoptotic BAX. Cell Rep. *30*, 3229–3239.e6.

Cowan, A.D., Smith, N.A., Sandow, J.J., Kapp, E.A., Rustam, Y.H., Murphy, J.M., Brouwer, J.M., Bernardini, J.P., Roy, M.J., Wardak, A.Z., et al. (2020). BAK core dimers bind lipids and can be bridged by them. Nat. Struct. Mol. Biol. *27*, 1024–1031.

Czabotar, P.E., Westphal, D., Dewson, G., Ma, S., Hockings, C., Fairlie, W.D., Lee, E.F., Yao, S., Robin, A.Y., Smith, B.J., et al. (2013). Bax crystal structures reveal how BH3 domains activate Bax and nucleate its oligomerization to induce apoptosis. Cell *152*, 519–531.

Dengler, M.A., Robin, A.Y., Gibson, L., Li, M.X., Sandow, J.J., Iyer, S., Webb, A.I., Westphal, D., Dewson, G., and Adams, J.M. (2019). BAX activation: mutations near its proposed non-canonical BH3 binding site reveal allosteric changes controlling mitochondrial association. Cell Rep. *27*, 359–373.e6.

Dewson, G., Ma, S., Frederick, P., Hockings, C., Tan, I., Kratina, T., and Kluck, R.M. (2012). Bax dimerizes via a symmetric BH3:groove interface during apoptosis. Cell Death Differ. *19*, 661–670.

Frohlich, M., Dejanovic, B., Kashkar, H., Schwarz, G., and Nussberger, S. (2014). S-palmitoylation represents a novel mechanism regulating the mitochondrial targeting of BAX and initiation of apoptosis. Cell Death Dis. *5*, e1057.

Garner, T.P., Amgalan, D., Reyna, D.E., Li, S., Kitsis, R.N., and Gavathiotis, E. (2019). Small-molecule allosteric inhibitors of BAX. Nat. Chem. Biol. *15*, 322–330.

Garner, T.P., Reyna, D.E., Priyadarshi, A., Chen, H.C., Li, S., Wu, Y., Ganesan, Y.T., Malashkevich, V.N., Cheng, E.H., and Gavathiotis, E. (2016). An autoinhibited dimeric form of BAX regulates the BAX activation pathway. Mol. Cell *63*, 485–497.

Gavathiotis, E., Reyna, D.E., Bellairs, J.A., Leshchiner, E.S., and Walensky, L.D. (2012). Direct and selective small-molecule activation of proapoptotic BAX. Nat. Chem. Biol. *8*, 639–645.

Gavathiotis, E., Reyna, D.E., Davis, M.L., Bird, G.H., and Walensky, L.D. (2010). BH3-triggered structural reorganization drives the activation of proapoptotic BAX. Mol. Cell *40*, 481–492.

Gavathiotis, E., Suzuki, M., Davis, M.L., Pitter, K., Bird, G.H., Katz, S.G., Tu, H.C., Kim, H., Cheng, E.H., Tjandra, N., et al. (2008). BAX activation is initiated at a novel interaction site. Nature *455*, 1076–1081.

Gross, A., Jockel, J., Wei, M.C., and Korsmeyer, S.J. (1998). Enforced dimerization of BAX results in its translocation, mitochondrial dysfunction and apoptosis. EMBO J. *17*, 3878–3885.

Hauseman, Z.J., Harvey, E.P., Newman, C.E., Wales, T.E., Bucci, J.C., Mintseris, J., Schweppe, D.K., David, L., Fan, L., Cohen, D.T., et al. (2020). Homogeneous oligomers of pro-apoptotic BAX reveal structural determinants of mitochondrial membrane permeabilization. Mol. Cell *79*, 68–83.e7.

Hsu, Y.T., Wolter, K.G., and Youle, R.J. (1997). Cytosol-to-membrane redistribution of Bax and Bcl-X(L) during apoptosis. Proc. Natl. Acad. Sci. U S A *94*, 3668–3672.

Hsu, Y.T., and Youle, R.J. (1998). Bax in murine thymus is a soluble monomeric protein that displays differential detergent-induced conformations. J. Biol. Chem. *273*, 10777–10783.

Ivashyna, O., Garcia-Saez, A.J., Ries, J., Christenson, E.T., Schwille, P., and Schlesinger, P.H. (2009). Detergent-activated BAX protein is a monomer. J. Biol. Chem. *284*, 23935–23946.

Kim, H., Tu, H.C., Ren, D., Takeuchi, O., Jeffers, J.R., Zambetti, G.P., Hsieh, J.J., and Cheng, E.H. (2009). Stepwise activation of BAX and BAK by tBID, BIM, and PUMA initiates mitochondrial apoptosis. Mol. Cell *36*, 487–499.

Kuwana, T., Mackey, M.R., Perkins, G., Ellisman, M.H., Latterich, M., Schneiter, R., Green, D.R., and Newmeyer, D.D. (2002). Bid, Bax, and lipids cooperate to form supramolecular openings in the outer mitochondrial membrane. Cell *111*, 331–342.

Leshchiner, E.S., Braun, C.R., Bird, G.H., and Walensky, L.D. (2013). Direct activation of full-length proapoptotic BAK. Proc. Natl. Acad. Sci. U S A *110*, E986–E995.

Li, H., Zhu, H., Xu, C.J., and Yuan, J. (1998). Cleavage of BID by caspase 8 mediates the mitochondrial damage in the Fas pathway of apoptosis. Cell *94*, 491–501.

Luna-Vargas, M.P.A., Mohammed, J.N., Gelles, J.D., and Chipuk, J.E. (2019). Mitochondrial isolation and real-time monitoring of MOMP. Methods Mol. Biol. *1877*, 121–130.

Meijerink, J.P., Mensink, E.J., Wang, K., Sedlak, T.W., Sloetjes, A.W., de Witte, T., Waksman, G., and Korsmeyer, S.J. (1998). Hematopoietic malignancies demonstrate loss-of-function mutations of BAX. Blood *91*, 2991–2997.

Mignard, V., Lalier, L., Paris, F., and Vallette, F.M. (2014). Bioactive lipids and the control of Bax pro-apoptotic activity. Cell Death Dis. *5*, e1266.

Mohammed, J.N., Gelles, J.D., and Chipuk, J.E. (2022). FLAMBE: A kinetic fluorescence polarization assay to study activation of monomeric BAX. STAR Protocols. https://doi.org/10.1016/j.xpro.2022.101252.

Niu, X., Brahmbhatt, H., Mergenthaler, P., Zhang, Z., Sang, J., Daude, M., Ehlert, F.G.R., Diederich, W.E., Wong, E., Zhu, W., et al. (2017). A small-molecule inhibitor of Bax and Bak oligomerization prevents genotoxic cell death and promotes neuroprotection. Cell Chem. Biol. *24*, 493–506.e5.

O'Neill, K.L., Huang, K., Zhang, J., Chen, Y., and Luo, X. (2016). Inactivation of prosurvival Bcl-2 proteins activates Bax/Bak through the outer mitochondrial membrane. Genes Dev. *30*, 973–988.

Perez, D., and White, E. (2000). TNF-alpha signals apoptosis through a bid-dependent conformational change in Bax that is inhibited by E1B 19K. Mol. Cell *6*, 53–63.

Pritz, J.R., Wachter, F., Lee, S., Luccarelli, J., Wales, T.E., Cohen, D.T., Coote, P., Heffron, G.J., Engen, J.R., Massefski, W., et al. (2017). Allosteric sensitization of proapoptotic BAX. Nat. Chem. Biol. *13*, 961–967.

Renault, T.T., Floros, K.V., and Chipuk, J.E. (2013). BAK/BAX activation and cytochrome c release assays using isolated mitochondria. Methods *61*, 146–155.

Renault, T.T., Floros, K.V., Elkholi, R., Corrigan, K.A., Kushnareva, Y., Wieder, S.Y., Lindtner, C., Serasinghe, M.N., Asciolla, J.J., Buettner, C., et al. (2015). Mitochondrial shape governs BAX-induced membrane permeabilization and apoptosis. Mol. Cell *57*, 69–82.

Reyna, D.E., Garner, T.P., Lopez, A., Kopp, F., Choudhary, G.S., Sridharan, A., Narayanagari, S.R., Mitchell, K., Dong, B., Bartholdy, B.A., et al. (2017). Direct activation of BAX by BTSA1 overcomes apoptosis resistance in acute myeloid leukemia. Cancer Cell *32*, 490–505.e10.

Ryan, J., and Letai, A. (2013). BH3 profiling in whole cells by fluorimeter or FACS. Methods *61*, 156–164.

Sarosiek, K.A., Chi, X., Bachman, J.A., Sims, J.J., Montero, J., Patel, L., Flanagan, A., Andrews, D.W., Sorger, P., and Letai, A. (2013). BID preferentially activates BAK while BIM preferentially activates BAX, affecting chemotherapy response. Mol. Cell *51*, 751–765.

Schafer, B., Quispe, J., Choudhary, V., Chipuk, J.E., Ajero, T.G., Du, H., Schneiter, R., and Kuwana, T. (2009). Mitochondrial outer membrane proteins assist Bid in Bax-mediated lipidic pore formation. Mol. Biol. Cell *20*, 2276–2285.

Schinzel, A., Kaufmann, T., Schuler, M., Martinalbo, J., Grubb, D., and Borner, C. (2004). Conformational control of Bax localization and apoptotic activity by Pro168. J. Cell Biol. *164*, 1021–1032.

Shamas-Din, A., Satsoura, D., Khan, O., Zhu, W., Leber, B., Fradin, C., and Andrews, D.W. (2014). Multiple partners can kiss-and-run: Bax transfers between multiple membranes and permeabilizes those primed by tBid. Cell Death Dis. *5*, e1277.

Subburaj, Y., Cosentino, K., Axmann, M., Pedrueza-Villalmanzo, E., Hermann, E., Bleicken, S., Spatz, J., and Garcia-Saez, A.J. (2015). Bax monomers form dimer units in the membrane that further self-assemble into multiple oligomeric species. Nat. Commun. *6*, 8042.

Sundararajan, R., and White, E. (2001). E1B 19K blocks Bax oligomerization and tumor necrosis factor alpha-mediated apoptosis. J. Virol. *75*, 7506–7516.

Sung, T.C., Li, C.Y., Lai, Y.C., Hung, C.L., Shih, O., Yeh, Y.Q., Jeng, U.S., and Chiang, Y.W. (2015). Solution structure of apoptotic BAX oligomer: oligomerization likely precedes membrane insertion. Structure *23*, 1878–1888.

Suzuki, M., Youle, R.J., and Tjandra, N. (2000). Structure of Bax: coregulation of dimer formation and intracellular localization. Cell *103*, 645–654.

Tan, C., Dlugosz, P.J., Peng, J., Zhang, Z., Lapolla, S.M., Plafker, S.M., Andrews, D.W., and Lin, J. (2006). Auto-activation of the apoptosis protein Bax increases mitochondrial membrane permeability and is inhibited by Bcl-2. J. Biol. Chem. *281*, 14764–14775.

Tsai, C.J., Liu, S., Hung, C.L., Jhong, S.R., Sung, T.C., and Chiang, Y.W. (2015). BAX-induced apoptosis can be initiated through a conformational selection mechanism. Structure *23*, 139–148.

Vasquez-Montes, V., Rodnin, M.V., Kyrychenko, A., and Ladokhin, A.S. (2021). Lipids modulate the BH3-independent membrane targeting and activation of BAX and Bcl-xL. Proc. Natl. Acad. Sci. U S A *118*, e2025834118.

Wang, K., Yin, X.M., Chao, D.T., Milliman, C.L., and Korsmeyer, S.J. (1996). BID: a novel BH3 domain-only death agonist. Genes Dev. *10*, 2859–2869.

Xin, M., Li, R., Xie, M., Park, D., Owonikoko, T.K., Sica, G.L., Corsino, P.E., Zhou, J., Ding, C., White, M.A., et al. (2014). Small-molecule Bax agonists for cancer therapy. Nat. Commun. *5*, 4935.

Yao, S., Westphal, D., Babon, J.J., Thompson, G.V., Robin, A.Y., Adams, J.M., Colman, P.M., and Czabotar, P.E. (2014). NMR studies of interactions between Bax and BH3 domain-containing peptides in the absence and presence of CHAPS. Arch. Biochem. Biophys. *545*, 33–43.

Zhai, D., Godoi, P., Sergienko, E., Dahl, R., Chan, X., Brown, B., Rascon, J., Hurder, A., Su, Y., Chung, T.D., et al. (2012). High-throughput fluorescence polarization assay for chemical library screening against anti-apoptotic Bcl-2 family member Bfl-1. J. Biomol. Screen. *17*, 350–360.

Zhang, H., Nimmer, P., Rosenberg, S.H., Ng, S.C., and Joseph, M. (2002). Development of a high-throughput fluorescence polarization assay for Bcl-x(L). Anal. Biochem. *307*, 70–75.

Zhang, Z., Subramaniam, S., Kale, J., Liao, C., Huang, B., Brahmbhatt, H., Condon, S.G., Lapolla, S.M., Hays, F.A., Ding, J., et al. (2016). BH3-in-groove dimerization initiates and helix 9 dimerization expands Bax pore assembly in membranes. EMBO J. *35*, 208–236.

STAR★METHODS

KEY RESOURCES TABLE

REAGENT or RESOURCE	SOURCE	IDENTIFIER
Antibodies		
BAX (2D2)	Santa Cruz Biotechnology	Cat# sc-20067; RRID: AB_626726
m-IgGκ BP-HRP	Santa Cruz Biotechnology	Cat# sc-516102; RRID: AB_2687626
Bacterial and virus strains		
One Shot BL21 (DE3) Chemically Competent *E. coli*	Thermo Fisher Scientific	Cat# C600003
Chemicals, peptides, and recombinant proteins		
2*t*-hexadecenal (16:1 aldehyde)	Avanti Polar Lipids	Cat# 857459
(3-cholamidopropyl)dimethylammonio)-1-propanesulfonate (CHAPS)	Gold Biotechnology	Cat# C-080
4-phenoxyphenol (BIF44)	Sigma Aldrich	Cat# 230669
8-aminonapthalene-1,3,6-trisulfonic acid (ANTS)	Thermo Fisher Scientific	Cat# A350
Alexa Fluor 488 C_5 Maleimide	Thermo Fisher Scientific	Cat# A10254
Alexa Fluor 660 NHS Ester	Thermo Fisher Scientific	Cat# A20007
BAI1 (≥99%)	Selleck Chemicals	Cat# S8865
Brain phosphatidylserine (Porcine)	Avanti Polar Lipids	Cat# 840032C
Cardiolipin (18:1)	Avanti Polar Lipids	Cat# 710335C
Chitin bead resin	New England Biolabs	Cat# S6651
Dichloro(1,10-Phenanthroline) Copper (II)	Sigma Aldrich	Cat# 362204
Disuccinimidyl suberate (DSS)	Thermo Fisher Scientific	Cat# 21655
Dodecylphosphocholine (≥95%)	Cayman Chemical	Cat# 25629
Egg phosphatidylcholine (Chicken)	Avanti Polar Lipids	Cat# 840051C
Egg phosphatidylethanoloamine (Chicken)	Avanti Polar Lipids	Cat# 840021C
Gel filtration standard	Bio-Rad	Cat# 1511901
Human BAK-BH3	AnaSpec	Cat# AS-61616
Human BAK-BH3, 5-TAMRA labeled	AnaSpec	Cat# AS-64590
Human BID-BH3	AnaSpec	Cat# AS-61711
Human BIM-BH3, Peptide IV	AnaSpec	Cat# AS-62279
Isopropyl-β-D-thiogalactoside (IPTG)	Gold Biotechnology	Cat# I2481C
Liver phosphatidylinositol (Bovine)	Avanti Polar Lipids	Cat# 840042C
n-octyl-β-D-glucoside	Thermo Fisher Scientific	Cat# 28310
p-xylene-bis-pyridinium bromide (DPX)	Thermo Fisher Scientific	Cat# X1525
Recombinant Human BAX	Chipuk Lab	Accession: NP_620116
Recombinant Human BID (Caspase-8-cleaved)	R&D Systems	Cat# 882-B8
Critical commercial assays		
CloneAmp HiFi PCR Premix	Takara Bio	Cat# 639298
QIAquick PCR Purification Kit	Qiagen	Cat# 28104
Oligonucleotides		
pTYB1-BAX^{V83C} mutagenesis primers: (forward) 5'- AGGAT GATTGCCGCCTGCGACACAGACTCCCCC-3', (reverse) 5'- GGGGGAGTCTGTGTCGCAGGCGGCAATCATCCT-3'	This paper	N/A
pTYB1-BAX^{G108V} mutagenesis primers: (forward) 5'- GCAA CTTCAACTGGGTCCGGGTTGTCGCCCT-3', (reverse) 5'- AGGGCGACAACCCGGACCCAGTTGAAGTTGC-3'	This paper	N/A
pTYB1-BAX^{R109D} mutagenesis primers: (forward) 5'- AACT TCAACTGGGGCGACGTTGTCGCCCTTTTC-3', (reverse) 5'- GAAAAGGGCGACAACGTCGCCCCAGTTGAAGTT-3'	This paper	N/A

(*Continued on next page*)

Continued

REAGENT or RESOURCE	SOURCE	IDENTIFIER
pTYB1-BAX^{I133A} mutagenesis primers: (forward) 5'-CAAG GTGCCGGAACTGGCCAGAACCATCATGGGC-3', (reverse) 5'-GCCCATGATGGTTCTGGCCAGTTCCGGCACCTTG-3'	This paper	N/A
pTYB1-BAX^{L185C} mutagenesis primers: (forward) 5'- GTGC TCACCGCCTCGTGCACCATCTGGAAGAA-3', (reverse) 5'- TTCTTCCAGATGGTGCACGAGGCGGTGAGCAC-3'	This paper	N/A
Recombinant DNA		
pTYB1-BAX^{A112C,V177C}	Evripidis Gavathiotis, Albert Einstein College of Medicine, NY, USA; Gavathiotis et al., 2010	N/A
pTYB1-BAX^{V83C,A112C,V177C,L185C}	This paper	N/A
pTYB1-BAX^{C62S,C126S}	Chipuk Lab	N/A
pTYB1-BAX^{C62S,V121C,C126S,I136C}	Chipuk Lab, Czabotar et al., 2013	N/A
pTYB1-BAX^{I133A}	Chipuk Lab, Dengler et al., 2019	N/A
pTYB1-BAX^{K21E}	Evripidis Gavathiotis, Albert Einstein College of Medicine, NY, USA; Gavathiotis et al., 2008	N/A
pTYB1-BAX^{L45C,M137C}	Evripidis Gavathiotis, Albert Einstein College of Medicine, NY, USA; Gavathiotis et al., 2010	N/A
pTYB1-BAX^{WT}	Chipuk Lab, Suzuki et al., 2000	N/A
Software and algorithms		
Excel v16.53.12091200	Microsoft	
Gen5 v3.10	Biotek	
ImageJ/Fiji v2.1.0/1.53c	National Institutes of Health	
Prism v9.2.0	Graphpad Software	
PyMOL v2.5.0	Schrödinger	
Other		
Amicon Ultra-15 Centrifugal Filter Units	EMD Millipore	Cat# UFC901024
Cytation 5 multi-mode plate reader	Agilent/BioTek	
Extruder Set (for large unilamellar vesicles)	Avanti Polar Lipids	Cat# 610023
HiLoad 16/600 Superdex 200 pg SEC column	Cytiva	Cat# 28989335
LUV Buffer (10 mM HEPES [pH 7], 200 mM KCl, 5 mM MgCl2, 0.2 mM EDTA)	N/A	N/A
Polycarbonate Membrane (1 μM)	Avanti Polar Lipids	Cat# 610010
Superdex 75 Increase 10/300 GL SEC column	Cytiva	Cat# 29148721
Synergy H1 Hybrid multi-mode plate reader	Agilent/BioTek	

RESOURCE AVAILABILITY

Lead contact

Further information and requests for resources and reagents should be directed to and fill be fulfilled by the lead contact, Jerry E. Chipuk (jerry.chipuk@mssm.edu).

Materials availability

Plasmids generated in this study are available upon request to the lead contact.

Data and code availability

- All data reported in this paper will be shared by the lead contact upon request.
- This paper does not report original code.
- Any additional information required to reanalyze the data reported in this paper is available from the lead contact upon request.

EXPERIMENTAL MODEL AND SUBJECT DETAILS

Bacterial cell lines

One Shot® BL21 (DE3) Chemically Competent *E. coli* were purchased from Invitrogen/Thermo Fisher Scientific (Cat. No. C600003). Cells were grown in BD Difco™ Terrific Broth (Cat. No. BD243820, Thermo Fisher Scientific) media supplemented with 1% glycerol at 37°C with shaking at 220 rpm.

METHOD DETAILS

Site-directed mutagenesis

BAX mutants used for bacterial expression were generated by site-directed mutagenesis of the original pTYB1-BAX construct (cDNA of human BAX inserted into NdeI/SapI site of pTYB1) (Suzuki et al., 2000). Amplification of the *de novo* plasmids was accomplished using CloneAmp HiFi PCR Premix (Cat. No. 639298, Takara Bio, Mountain View, CA, USA) and thermocycled as follows: 1× 98°C for 2 min; 30× 98°C for 10 sec, 55°C for 30 sec, 72°C for 8 min; and 1× 72°C for 10 min. Parental plasmids were digested by 1 μl DpnI enzyme (Cat. No. R0176, New England Biolabs, Ipswich, MA, USA) at 37°C for 15 minutes, followed by purification using the QIAquick PCR Purification Kit (Cat. No. 28104, Qiagen, Hilden, Germany). Sequences were verified using the Genewiz Universal T7 primer (5'-TAATACGACTCACTATAGGG-3'). Plasmids for the expression of $BAX^{\alpha 9}$, $BAX^{\beta 1-2}$, and BAX^{K21E} were generously provided by Dr. Evripidis Gavathiotis (Albert Einstein College of Medicine, Bronx, NY, USA).

BAX purification, recombinant proteins, and peptides

Recombinant human BAX was expressed and purified using an intein tag as originally described (Suzuki et al., 2000). pTYB1-BAX was transformed into and expressed in *E. coli* BL21(DE3) cells and cultured in Terrific Broth media at 37°C. Once bacterial cultures reached an OD600 value between 2–3 (approximately 4–5 hours), protein expression was induced with 1 mM IPTG at 30°C for 6 hours. Bacteria cells were harvested, lysed by sonication for 20 minutes in lysis buffer (50 mM K_2PO_4, 50 mM NaH_2PO_4, 500 mM NaCl, 1 mM EDTA, 0.1 mM AEBSF) supplemented with a Pierce protease inhibitor tablet (Cat. No. A32965, Thermo Scientific), and centrifuged at 39,400*g* at 4°C for 1 hour. Intein-tagged recombinant human BAX was isolated from the supernatant by chitin affinity chromatography according to the manufacturer's protocol (Cat. No. S5551, New England Biolabs, Ipswich, MA, USA). On-column intein cleavage was achieved by overnight incubation with DTT (50 mM) at 4°C, and BAX was eluted with Gel Filtration buffer (20 mM HEPES [pH 7.4], 150 mM NaCl). BAX was further purified by size-exclusion chromatography on a HiLoad 16/600 Superdex 200 pg column (Cat. No. 28989335, Cytiva) using an ÄKTA pure 25 L1 (Cat. No. 29018225, Cytiva). Peak fractions containing recombinant BAX protein were combined and concentrated (to 20–30 μM) using Amicon Ultra-15 centrifugal filter (Cat. No. UFC901024, EMD Millipore) prior to snap freezing and storage at -80°C. Nascent BAX mutants were purified in the reduced form due to DTT incubation during intein cleavage. To generate disulfide tethers, BAX mutants were oxidized in 1 mM Dichloro(1,10-Phenanthroline) Copper (II) (Cat. No. 362204, Sigma-Aldrich) at 4°C for 15 minutes, purified by Superdex 75 Increase 10/300 GL column (Cat. No. 29148721, Cytiva), and only monomeric species were taken to make protein stocks.

Additional recombinant proteins and peptides were purchased from commercial sources: BAK-BH3 (Cat. No. AS-61616, AnaSpec); BAK-BH3, 5-TAMRA labeled BAK-BH3 (Cat. No. AS-64590, AnaSpec); BID-BH3 (Cat. No. AS-61711, AnaSpec); BIM-BH3, Peptide IV (Cat. No. AS-62279, AnaSpec); Caspase-cleaved recombinant BID (Cat. No. 882-B8, R&D Systems). Of note, BIM^{BH3} reagents exhibit markedly different efficacies of BAX activation due to structure, sequence, and length differences. In this work, we observed a significant reduction in BAX activation when we replaced the 26-mer BIM^{BH3} peptide (aa 141–166, "Peptide IV", AnaSpec #AS-62279) with a 25-mer peptide (aa 141–165, "Peptide III", AnaSpec #AS-62278) spanning the same region of BIM (data not shown). Similarly, investigators utilizing the stapled α-helical BIM peptide (BIM $SAHB_A$) should note that there are two varieties (aa 145–164 and aa 146–166), which exhibit different potencies due to disparities in α-helicity and charge (Bird et al., 2014).

Fluorescence polarization assay and data parameterization

Assay setup

Working stocks of recombinant proteins, peptides, or detergents were prepared for BAX studies by diluting each component in 0.5× PBS. Components were combined in a black polystyrene 96-well plate in the following volumes for a 100 μl final volume: 50 μl titrant stock, 25 μl BAX stock, 25 μl BAK^{TAMRA} stock. Typical assays were prepared as follows: 1) titrations were generated via in-well serial dilutions and buffer was added to any control wells requiring volume compensation; 2) BAX was added to appropriate wells using a multichannel pipet to prevent excessive delays due to pipetting; 3) the final component added to wells was BAK^{TAMRA}, pipetted with a multichannel to reduce delays; 4) immediately following addition of BAK^{TAMRA} (t=0), plates were subjected to spectrometry for 1 hour using a Synergy H1 hybrid multi-mode microplate reader (BioTek, Winooski, VT, USA) fit with a polarization filter using parameters listed in Table: Parameters for fluorescence polarization assay. Polarization (expressed as milli-Polarization (mP) units) is derived from measured parallel and perpendicular emission intensities (I) by the BioTek Gen5 software according to the following equation:

$$\mathrm{mP} = \frac{(I_{parallel} - I_{perpendicular})}{(I_{parallel} + I_{perpendicular})} \times 1000$$

Ideal concentrations of recombinant BAX protein for assays were determined by extensive titrations and re-evaluated for each preparation of recombinant protein. Typically, the highest BAX concentration exhibiting no auto-activation was selected for activation studies. Similarly, concentrations of direct activators, detergents, or small molecule BAX modulators were selected from extensive titration experiments to determine appropriate concentrations for each experimental setup (e.g., activating or sub-activating conditions). In each experiment, the BAK^{TAMRA} control is shown in grey. A more detailed step-by-step protocol has been co-published in *STAR Protocols* (Mohammed et al., 2022).

Kinetic FP data parameterization

Parameterized FP data was derived from the average of replicates to reduce data noise. For each condition, T_{max} was identified as the timepoint with the highest Polarization and Endpoint was the final Polarization value recorded. T_{max} of the BAK^{TAMRA} control or any sample exhibiting no binding kinetics during the assay was set as 0 to avoid misidentification due to data noise. Each parameterized metric was normalized to metrics from the BAK^{TAMRA} and BAX control conditions as 0 and 1, respectively.

Assay limitations

Even minor delays in reading the plate following addition of components negatively affected data collection and resulted in decreased resolution of association curves. Similarly, the number of wells included in each assay did not exceed 24 wells to ensure rapid scan intervals for kinetic data density. Kinetic data represent the mean of duplicate samples and are representative of at least three repeated and reproduced assays using separate protein aliquots. Assays could not be run in triplicate due to the added time of pipetting the BAK^{TAMRA}, which introduced enough time that replicates had different t=0 timepoints and kinetic curves were shifted across replicates.

Table: Parameters for fluorescence polarization assay

Reader	BioTek synergy H1 hybrid multi-mode plate reader
Filter cube	red FP polarizer filter set (#8040562)
Read interval	30–60 s
Total read time	60 min
Protocol	25°C; 3 s linear shake; read
Excitation	530/25 nm
Emission	590/35 nm
Gain (voltage)	50
Optics position	top, 570 nm
Read height	7.0 mm
Assay plate	black polystyrene 96-well (Corning #3915)
Assay buffer	0.5× PBS (or LUV buffer for tandem assays)

Large unilamellar vesicle (LUV) permeabilization assays

LUV composition and generation

Large unilamellar vesicles (LUVs) and permeabilization assays were prepared as similarly described (Asciolla et al., 2012; Kuwana et al., 2002). Briefly, chicken egg phosphatidylcholine (Cat. No. 840051C, Avanti Polar Lipids), chicken egg phosphatidylethanoloamine (Cat. No. 840021C, Avanti Polar Lipids), porcine brain phosphatidylserine (Cat. No. 840032C, Avanti Polar Lipids), bovine liver phosphatidylinositol (Cat. No. 840042C, Avanti Polar Lipids), and cardiolipin (18:1) (Cat. No. 710335C, Avanti Polar Lipids) were combined at a ratio of 48:28:10:10:4 (5 mg total), dried under N_2 gas, and resuspended in LUV buffer (10 mM HEPES [pH 7], 200 mM KCl, 5 mM $MgCl_2$, 0.2 mM EDTA) containing a polyanionic dye (12.5 mM ANTS: 8-aminonaphthalene-1,3,6-trisulfonic acid) and cationic quencher (45 mM DPX: *p*-xylene-bis-pyridinium bromide) using a water bath sonicator. Unilamellar vesicles were formed by extrusion of the suspension through a 1.0 μm polycarbonate membrane (Cat. No. 610010, Avanti Polar Lipids, Alabaster, AL, USA). The unincorporated DPX and ANTS were removed by using a 10 ml Sepharose CL-2B gravity flow column. LUV preparations were only used for <2 weeks from when they were generated to avoid significant liposome degradation.

LUV assays

Using a 96 well format and 100 μl total volume per condition, LUVs, proteins, peptides, and buffers were combined as indicated and analyzed for fluorescence using a Cytation 5 multi-mode microplate reader (BioTek, Winooski, VT, USA) using parameters listed in Table: Parameters for LUV permeabilization assay. Kinetic data represent the mean of triplicate samples and are representative of at least three repeated and reproduced assays using separate protein aliquots. Every assay contained a 1% CHAPS control to determine maximum signal and these data are shown in grey. Normalized endpoint data (% permeabilization) was calculated in Prism (Graphpad) using the minimum value of the buffer control (as 0%) and the maximum value of LUVs solubilized in 1% CHAPS

(as 100%) measured during the entire assay. Recombinant BAX protein concentrations were determined by extensive titrations, and the lowest concentration for maximal activity for each protein was used, and this was determined for each preparation of recombinant protein and LUVs. For FP-LUV tandem assays, FP samples were prepared and measured in LUV buffer as described above; following completion of the FP assay, 5 μl of LUVs were immediately added to each well and kinetically measured for permeabilization-associated fluorescence according to a standard LUV assay. Every tandem assay included BAK^{TAMRA} and BAK^{TAMRA}+LUV controls to confirm no substantial contribution to signal accumulation or LUV permeabilization.

Table: Parameters for LUV permeabilization assay

Reader	BioTek Cytation 5 Multi-Mode Plate Reader
Read interval	55 seconds
Total read time	90 minutes
Protocol	37°C; 2 second linear shake; read
Excitation	355/25 nm
Emission	520/35 nm
Gain (voltage)	100
Optics Position	Top, 570 nm
Read Height	5.5 mm
Assay Plate	Black polystyrene 96-well (Corning #3915)
LUV buffer	10 mM HEPES (pH 7), 200 mM KCl, 5 mM $MgCl_2$, 0.2 mM EDTA

Cross-linking, gel electrophoresis, and immunoblotting

Protein crosslinking was performed at a concentration of 125 μM DSS (or DMSO control) at 25°C for 30 minutes. The cross-linker was quenched by the addition of Tris-HCl (pH 8) to a final concentration of 1.25 mM. Samples were combined with 1× Laemmli buffer supplemented with DTT, subjected to SDS-PAGE in a 10% polyacrylamide gel, and transferred to nitrocellulose by standard western blot conditions. Membranes were blocked in 5% milk/TBST, incubated with primary antibodies (1:1000 in blocking buffer; incubated 4°C overnight) and secondary antibodies (1:5000 in blocking buffer; incubated for 1 hour at 25°C), followed by standard enhanced chemiluminescence detection. Native-PAGE samples were composed of 100 ng BAX co-incubated as indicated overnight at 4°C. Samples were mixed with 2× native sample buffer (Cat. No. 1610738, Bio-Rad), run on a 15% polyacrylamide gel, transferred to nitrocellulose by standard western blot conditions, and probed as described above. Molecular weight markers were inferred using recombinant GST, which ran as monomeric and dimeric species. Primary antibody: BAX (2D2, Cat. No. sc-20067, Santa Cruz Biotechnology); secondary antibody: m-IgGκ BP-HRP (Cat. No. sc-516102, Santa Cruz Biotechnology). Of note, this BAX antibody displays increased sensitivity for oligomeric species.

Size-exclusion chromatography and quantification of band intensities

Gel filtration was performed by Superdex Increase 75 10/300 column (Cat. No. 29148721, Cytiva) using ÄKTA pure 25 L1 (Cat. No. 29018225, Cytiva). 35 μg of purified BAX was incubated at 4°C overnight with indicated treatments in 700 μl. 500 μl of the reaction volume was injected onto the column, collected in 0.5 ml fractions, and 15 μl of the fractions were subjected to SDS-PAGE. Molecular weight indicators were established using a standard (Cat. No. 1511901, Bio-Rad) and referenced for all future experiments. Quantification of western blots was measured in ImageJ/Fiji (National Institutes of Health, Bethesda, MD, USA) following global adjustments to brightness and contrast. Each band was bounded by a fixed-area box and quantified to generate a pixel intensity histogram. The area under the histogram was determined and used as a surrogate for band intensity. Raw histogram area values were expressed as a percentage of the total histogram area measured across all bands. In samples where BAX reformed dimeric species following denaturing, the dimer bands were quantified and these percentages are as stacked bars. Westerns and quantifications are representative of at least three repeated and replicated experiments.

Fluorescent gel filtration experiments

Peptide labeling and trichloroacetic acid (TCA) precipitation

Alexa Fluor 488 (AF488)-labeled BAX and Alexa Fluor 660 (AF660)-labeled BIM^{BH3} were generated according to the manufacturer's instructions (Invitrogen, Thermo Fisher Scientific) at 10:1 protein:dye molar excess and purified using G25 spin columns (BAX) or TCA precipitation (BIM^{BH3} peptide). Precipitation was carried out by adding TCA to a final concentration of 25%, incubating at 4°C for 1 hour, and pelleting by centrifugation at 21,000*g* for 5 minutes. Pelleted samples were decanted, washed twice with 200 μl 4°C acetone, dried by evaporation for 15–20 minutes, and resuspended in suitable buffers (Gel Filtration buffer for BAX, DMSO for BIM^{BH3}). Peptides were protected from light at each step.

Gel filtration and detection

Fluorescent proteins and peptides were incubated in 0.5× PBS for 1 hour at concentrations that replicated FLAMBE experiments, followed by size-exclusion chromatography as described above. Fractions were precipitated by adding 125 μl 100% TCA (1:4 volume ratio), processed as described above, and then solubilized in 100 μl of Gel Filtration buffer (20 mM HEPES [pH 7.4], 150 mM NaCl) containing 1% SDS with brief vortexing. Samples were transferred to a black polystyrene 96-well plate and analyzed for fluorescence by a Cytation 5 multi-mode plate reader (BioTek, Winooski, VT, USA) using read parameters detailed in Table: Parameters for fluorescent gel filtration measurements. Proteins are denatured in this preparation and therefore fluorescence would not be affected by peptide folding or interactions.

Table: Parameters for fluorescent gel filtration measurements

Channel (protein)	Excitation/bandpass	Emission/bandpass	Gain
Green (AF488-BAX)	495/10 nm	520/10 nm	100
Red (BAK^{TAMRA})	530/10 nm	590/10 nm	150
Far-red (AF660-BIM^{BH3})	662/10 nm	690/10 nm	150

BAX structure visualization and annotation

Human BAX structure was visualized with PyMOL (Schrödinger, New York, NY, USA) from PDB files 2K7W or 1F16 (Gavathiotis et al., 2008; Suzuki et al., 2000). Mutant BAX illustrations were recreated from visualizations generated by the PyMOL mutagenesis wizard to incorporate residue substitutions. Interaction site residues were defined according to published works or visual inspection of surface topology. The highlighted regions are as follows: BC groove (I66, G67, L70, L76, I80, V83, V91, R94, V95, D98, M99, G108, V111, A112, L113, Y115, F116, K119); trigger site (M20, K21, A24, L25, Q28, I31, Q32, R134, T135, M137, G138, L141, D142, R145); allosteric site (I80, A81, V83, D84, T85, D86, P88, V91, F92, L120, K123, A124, T127, L132, I136).

QUANTIFICATION AND STATISTICAL ANALYSIS

Polarization (expressed as milliPolarization units) was derived for each timepoint in real-time by the Gen5 v3.10 software (BioTek) from parallel and perpendicular intensity measurements. FLAMBE data parameterization was conducted with Excel v16.53.12091200 (Microsoft) using formulas to identify T_{max} and EP, though this is also achievable manually. Sample T_{max} and EP were normalized against the BAK^{TAMRA} control (set as 0) and the relevant BAX control (set as 1). Normalized LUV endpoint data was calculated using Prism v9.2 (Graphpad Software Inc.) with the minimum and maximum value from the buffer control (0%) and CHAPS-solubilized LUVs (as 100%) collected over the duration of the entire assay, respectively. Westerns were quantified using ImageJ/Fiji v2.1/1/53c (National Institutes of Health) by bounding bands with fixed-area boxes, generating pixel intensity histograms, and calculating the area under the histogram peak as a surrogate for band intensity. Raw histogram area values were expressed as a percent of the total histogram area measured for all bands. FP experiments were conducted in duplicate and LUV experiments were conducted in triplicate and data is presented as the mean of replicates. When shown, error bars denote standard deviation of replicates; kinetic data graphs omit error bars to aid in visualization. All data is representative and reproduced in experiments repeated at least three times.